INFORMATION TO USERS

While the most advanced technology has been used to photograph and reproduce this manuscript, the quality of the reproduction is heavily dependent upon the quality of the material submitted. For example:

- Manuscript pages may have indistinct print. In such cases, the best available copy has been filmed.

- Manuscripts may not always be complete. In such cases, a note will indicate that it is not possible to obtain missing pages.

- Copyrighted material may have been removed from the manuscript. In such cases, a note will indicate the deletion.

Oversize materials (e.g., maps, drawings, and charts) are photographed by sectioning the original, beginning at the upper left-hand corner and continuing from left to right in equal sections with small overlaps. Each oversize page is also filmed as one exposure and is available, for an additional charge, as a standard 35mm slide or as a 17"x 23" black and white photographic print.

Most photographs reproduce acceptably on positive microfilm or microfiche but lack the clarity on xerographic copies made from the microfilm. For an additional charge, 35mm slides of 6"x 9" black and white photographic prints are available for any photographs or illustrations that cannot be reproduced satisfactorily by xerography.

Xu, Jia

SURFACE ENHANCED RAMAN SPECTROSCOPY ON ELECTRODES: ENHANCEMENT MECHANISMS AND APPLICATION TO THE STUDIES OF FLAVIN MOLECULES

City University of New York PH.D. 1987

PLEASE NOTE:

In all cases this material has been filmed in the best possible way from the available copy. Problems encountered with this document have been identified here with a check mark __✓__.

1. Glossy photographs or pages _____
2. Colored illustrations, paper or print _____
3. Photographs with dark background _____
4. Illustrations are poor copy _____
5. Pages with black marks, not original copy _____
6. Print shows through as there is text on both sides of page _____
7. Indistinct, broken or small print on several pages __✓__
8. Print exceeds margin requirements _____
9. Tightly bound copy with print lost in spine _____
10. Computer printout pages with indistinct print _____
11. Page(s) _____ lacking when material received, and not available from school or author.
12. Page(s) _____ seem to be missing in numbering only as text follows.
13. Two pages numbered _____. Text follows.
14. Curling and wrinkled pages _____
15. Dissertation contains pages with print at a slant, filmed as received __✓__
16. Other _____

_____

_____

University
Microfilms
International

SURFACE ENHANCED RAMAN SPECTROSCOPY ON ELECTRODES: ENHANCEMENT MECHANISMS AND APPLICATION TO THE STUDIES OF FLAVIN MOLECULES

by

JIA XU

A dissertation submitted to the Graduate Faculty in Chemistry in partial fulfillment of the requirements for the degree of Doctor of Philosophy, The City University of New York.

1987

This manuscript has been read and accepted for the Graduate Faculty in Chemistry in satisfaction of the dissertation requirement for the degree of Doctor of Philosophy.

1/8/87
date

Chairman of Examining Committee

1/13/87
date

A. M.
Executive Officer

Supervisory Committee

The City University of New York

Abstract

SURFACE ENHANCED RAMAN SPECTROSCOPY ON ELECTRODES: ENHANCEMENT MECHANISMS AND APPLICATION TO THE STUDIES OF FLAVIN MOLECULES

by

JIA XU

Advisers: Professor Ronald L. Birke and Professor John R. Lombardi

A comprehensive development of the charge-transfer theory of surface enhanced Raman scattering (SERS) is presented. It was done by incorporating the Herzberg-Teller mixing of zero-order Born-Oppenheimer electronic states by means of vibronic interaction terms in the Hamiltonian. The theory is comprehensive in that both molecule-to-metal and metal-to-molecule transfer is considered. Furthermore, both Frank-Condon and Herzberg-Teller contributions to the intensity are obtained. The former, however, contribute only to the intensity of totally symmetric vibrations, while the latter contribute to nontotally symmetric vibrations as well. The resulting formulas may be interpreted as a type of resonance Raman effect in which intensity for the charge transfer transitions is borrowed from an allowed molecular transition. Based on this theory and the electromagnetic enhancement factors obtained from the small sphere model, the determination of molecular orientation at metal surfaces is discussed and applied for pyridine molecules on a Ag electrode at different potentials.

The surface enhanced Raman scattering (SERS) spectroscopy of protein-free flavin in different redox states was investigated at a silver electrode. Good quality spectra for oxidized flavin with an excitation frequency within the absorption band (488 or 514.5 nm) and out of the absorption band (yellow-red region) are reported. Fluorescence interference from the flavin is nearly completely quenched

by the surface interaction. The bonding sites of the flavin on a silver electrode appear to be at N_5 and O_4 positions of the isoalloxazine ring based upon the results of N_3-H deuterium substitution and from the SERS spectral analysis. Reduced flavin did not exhibit a well defined SERS spectrum, probably because of the break down of the surface complex. The SERS spectrum of the neutral semiquinone radical, as an intermediate of the two single electron reduction steps, was observed in acidic solution with yellow or red excitation. The utility of SERS as a technique for probing the existence of an unstable intermediate species at the electrode surface is demonstrated.

Table of Contents

List of Tables

List of Figures

CHAPTER 1

INTRODUCTION

An interface is the junction of two substances or of two phases of the same substance. The physics and chemistry of interfaces is becoming more and more important as an exciting field of basic research as well as in the development of devices and technology. One of four reports requested by the President's science advisers for "Research Briefings 1986" is addressed to this subject and titled as "Field of Interfaces and Thin Films Ripe for Discoveries" [1]. This current interest in interfaces reflects both timely opportunities in basic science and great pervasiveness in technology:

A broadly important problem in science is the basic relations between macroscopic properties of matter and atomic structure. Interfaces, of which the detailed structures can be manipulated with greater control than can those of bulk solid or liquids, provides particularly attractive systems with which to study these basic relations.

The structure, properties and reactivity of matter at an interface can be very different from those of matter in bulk. Technologically important physical and chemical properties, e.g., strength, corrosion resistance, biocompatibility, catalytic capability etc. are often determined by the characteristics of interfaces and thin films.

However, understanding and controlling interface properties have been difficult because of the small quantities of material present in most interfaces relative to the bulk, and because many of the interfaces of greatest interest are "buried" inside solids or under liquids. The bonding and electronic structure of

most interfaces are still poorly understood and no technique for establishing those structures is universally applicable. Much of the information about the structures of interfaces has come from forms of spectroscopy applicable only to solid-vacuum interfaces, such as high resolution electron energy loss (HREEL) [2], ultraviolet or X-ray photoelectron spectroscopy (UPS or XPS) [3,4], Auger electron spectroscopy (AES) [5] and secondary ion mass spectroscopy (SIM) [6,7]. Now, however, techniques capable for characterization of solid-gas, solid-liquid and solid-solid interfaces are emerging [1]. Surface enhanced Raman spectroscopy is one of these newly developed techniques.

In 1974, Fleishman, Hendra and McQuillan [8] observed Raman scattering from pyridine adsorbed on a roughened silver electrode in an electrochemical cell. In 1977, a calibration of the Raman signal from pyridine on silver electrode was made by Jeanmaire and Van Duyne [9] and independently by Creighton and Albrecht [10]. Both groups found that the Raman signal per adsorbed molecule was roughly six order of magnitude larger than that obtained from a molecule in solution. Soon after these initial reports the effect was also observed on colloidal [11,12], Ag island film [13], ultra high vacuum [14] and tunnel-junction [15,16] interfaces and was termed Surface Enhanced Raman Scattering (SERS). It is possibly the most sensitive (10^{-3} monolayer) surface high resolution (1 cm^{-1}) and wide region (100-4000 cm^{-1}) vibrational spectroscopic technique available for all material phases (vacuum, gas, liquid, and solid) in contact with certain metal surfaces [17]. A great interest was aroused in the physics, chemistry, and material science research communities to study SERS both as a fundamental phenomenon and as a new technique.

A large number of scientists with widely varying backgrounds and approaches joined in the quest for the enhancement mechanism. It has turn out to be difficult and exciting because at least two kinds of mechanisms, very different in their microscopic origins, appear to be involved in different proportions depending upon the systems under investigation [18-24]. These studies have been shown to be valuable not only for the understanding of SERS itself but, through it, the knowledge of the various forms of interaction among photons, molecules and metal surfaces in general.

This work is conducted using the metal-solution interface in an electrochemical cell. Its aim is to develop both a theoretical understanding of the phenomenon and an application of the SERS for determining the bonding structure of adsorbates and the electrochemical reaction mechanisms at an electrode surface. The experimental methods will be discussed in chapter 2. A detailed review on various theories is given in chapter 3 to describe and reveal the nature of the problems and to outline the present research themes. In chapter 4, a comprehensive development of the charge-transfer theory of SERS is presented together with a discussion on the variability of the total intensity of SERS as a function of excitation energy, applied potential and molecular orientation at the surface. The application of SERS to the study of the electron transfer mechanisms of flavin reduction reactions is demonstrated in chapter 5.

CHAPTER 2

EXPERIMENTAL METHODS

In this chapter a brief account is given of the equipment and the experimental procedures employed in this work, together with some general remarks regarding the oxidation-reduction cycle (ORC) pretreatment. A block diagram for the spectroelectrochemical apparatus sufficient to give SERS with a conventional photon counting apparatus and a computer interface, as used in our laboratory is shown in Figure 2-1. It consists of three major parts: (1) a laser radiation source, (2) a spectral detecting device, and (3) the electrochemical cell and instrumentation. The details of each part and the pretreatment procedures will now be described.

2.1 Laser Radiation Source and Optical Set-up

A continuous wave laser is used as the radiation source in the SERS experiments. A Spectra Physics 164 argon ion laser provides two strong (> 1 W) lines at 488 and 514.5 nm, and several moderate lines in the frequency region from 457.9 to 528.7 nm. are also produced. Laser lines between 550 and 630 nm are obtained with a Spectra Physics model 375 tunable dye laser excited by the argon ion laser. A Spectra Physics 2000 krypton ion laser gives a strong line at 647.1 nm. An interference filter is used to eliminate unwanted lasing lines from gaseous ion lasers. Alternatively, a grating can be used to spatially reject these lines. The laser beam is then focussed to a spot on the electrode surface.

A collection geometry is fixed at 90° angle between the incident light and the collected scattering light. The angle of incidence is varied by rotating the electrode on a x-y-z micro-positioner. Since monochromators have different sensitivities to

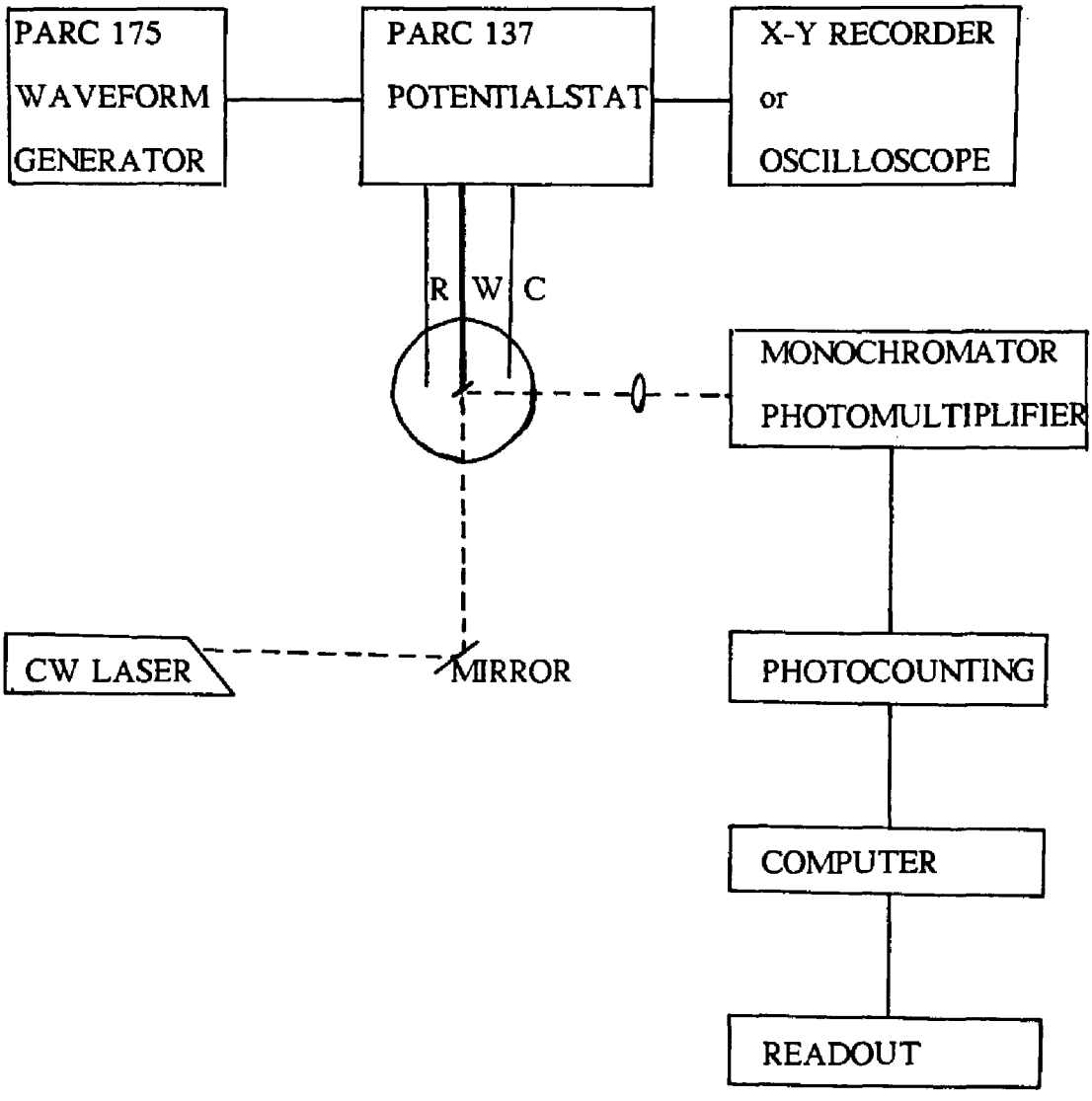

Figure 2-1 Block diagram of a spectroelectrochemical system for recording SERS.

light of different polarizations, a scrambler (calcite wedge) is placed in front of the entrance slit to scramble the polarization. The laser power on the electrode is usually set in the range of 20-100 mw.

2.2 The Monochromator and Detection System

2.2.1 Scanning monochromator

SPEX 1401 double monochromator is used to disperse the SERS light and a cooled FW' 130/72 photonmultiplier (PM) tube serves as the detector. The dispersion $d\lambda/dl$ (λ is wavelength and l is the slit width) is 1.31×10^{-6} and for a 50μ slit width and visible light, the resolution is ca. 2 cm^{-1}. The output anode pulses of the PM tube are fed to a low noise amplifier whose output then goes to a pulse-height discriminator. The pulse-height discriminator level is set to pick up the largest number of signal pulses while rejecting background (dark current) pulses. The shaped pulses are then counted by logical level digital counters which are interfaced to a laboratory digital computer. The spectrum could then be stored on magnetic medium and displayed through an oscilloscope monitor or in hard-copy form on a digital plotter or x-y recorder. This instrument gives accurate band positions and accurate relative intensities for a time stable spectrum.

2.2.2 Optical Multichannel Analyzer (OMA)

In order to suppress the grating scattering from the Rayleigh light, a triple monochromator is used where the front end is a double monochromator in a subtractive dispersion mode. This stage produces a non-dispersed spectrum rejecting nearly all of the Rayleigh scattered light. The final stage is a single grating monochromator which disperses the spectrum on a flat focal plane coupled to the detector.

The dispersed photons striking a multichannel detector produce a charge pattern in the diodes which can be periodically read out into an interfaced computer. The complete instrument is usually referred to as the Optical Multichannel Analyzer (OMA). The spectral range and resolution can be adjusted by changing the last grating. A 1200 gr/mm grating is usually used which gives a spectral region ca. 800 cm^{-1}. A wavelength calibration is done with the emission lines of a neon lamp. The Raman shift of recorded spectra is in wavelength which can be converted to wavenumbers by a computer program.

The use of an OMA device for recording SERS spectra has the advantage of not only fast recording of a single spectrum but also allowing successive spectra to be recorded as a function of time for kinetic studies or as a function of electrode potential for three dimensional recordings of SER intensity-cm^{-1}-potential plots.

2.3 The Electrochemical Cell and Instrumentation

A simply constructed electrochemical cell for SERS is shown in Figure 2-2. The bottom and one side of the cell are made with optically flat quartz windows. The working electrode potential is controlled with respect to a reference electrode by a potentiostat that provides current through the counter electrode. For aqueous electrolyte solutions, the counter electrode is a platinum wire and the reference electrode is a saturated calomel reference (SCE). The working electrode can be constructed from a 99.9995 pure SERS active metal wire (e.g. Ag, Au, and Cu) which is embedded in a teflon cylinder. The electrode is cut at 45° angle to facilitate the 90° scattering with the laser beam entering from the bottom of the cell. The cell has provisions for inert gas (N_2, Ar or He) bubbling for deoxygenation, a port for adding chemical species or flushing through blank electrolyte, and a port with a

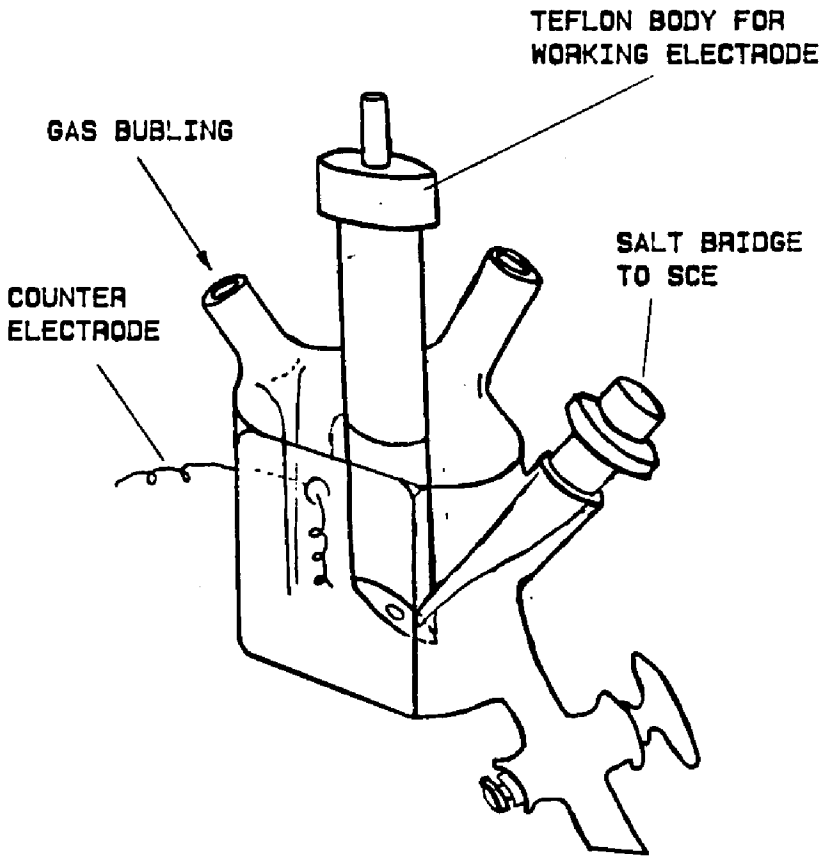

Figure 2-2. Electrochemical cell for SERS.

stopcock for removing solution while the cell is still positioned in the spectrometer. The latter feature is handy for flushing out the cell with blank electrolyte solution, while the working electrode is under potential control, without changing the optical alignment. This technique may be used to separate the Raman scattering of an irreversibly adsorbed species from that of an intense resonance Raman or from the fluorescence interference in solution.

Another way to eliminate the fluorescence interference from the solution is by placing the working electrode very close to the front window. The working electrode is put into the cell from the back. The light path from the electrode surface to the front window can be as short as 2 mm. With this cell, in-situ SERS studies of electrochemical reaction mechanism can be carried out for fluorescent molecules.

Working electrode potentials are controlled relative to the SCE by a potentiostat (PARC 173), which has a built-in coulometer (PARC 179) allowing the charge passed during an ORC pretreatment to be read out. Potential square waves or cyclic potential ramps can be applied to the potentiostat input from a waveform generator (PARC 175). Outputs from the waveform generator and the current follower circuit of the potentiostat are connected to the inputs of an x-y recorder or an oscilloscope (if the sweep rate is higher than 0.1 V/s) for recording the variations in the cell current with applied potential, i.e., cyclic voltamogram.

2.4 The Pretreatment and Electrochemical Measurement

The working electrode is first polished with a finely divided alumina (0.3 micron) slurry and then cleaned with deionized distilled water. The initial potential is set negative to the onset of silver oxidation and the electrode potential is

either stepped or swept to a potential where silver oxidation occurs. The dwell time at the positive limit is 1-5 seconds and a 20-50 mV/s scan rate is usually used in sweeping pretreatment. The up-limit and low-limit of an ORC depend on the oxidation potential of the metal in a given electrolyte solution. Some examples are listed in Table 2-1. Generally, the electrolyte anion should have a small K_{sp} with Ag^+ when the probe molecule is a cation or weakly adsorbed neutral molecule, whereas KNO_3 or K_2SO_4 is best used for an anion or a strongly adsorbed molecule. In the former case, such as pyridine and pyridinum, Cl^- ions will be coadsorbed with the sample molecule. In the latter case, however, Cl^- ions will compete with the sampling species in the adsorption so that, e.g., a better riboflavin SERS spectrum was obtained from K_2SO_4 solution than from KCl solution.

Illumination with laser light during ORC pretreatment gives an additional enhancement of as much as ten-fold in most cases. However, it often leads to larger irreproducibility, causing appearance of some new bands or spectral changes in relative intensity in some systems. In order to compare the SERS spectra of different excitation frequencies, the ORC pretreatment should be done in the dark.

When sample molecules are added after an ORC pretreatment to a pure electrolyte solution, the SERS spectrum obtained is usually much weaker than that from the one pretreated in the presence of the sample molecules. To avoid oxidation of the probe molecule during the ORC in some cases, a rough surface can be made by a direct reduction of the added Ag^+ ions in the sample solution. The SERS intensity is thus comparable with that obtained in the normal way.

Table 2-1. ORC Pretreatment of a Ag Electrode in Several Electrolyte Solutions

electrolyte(0.1 M)	K_{sp} with Ag^+	uplimit (V)	Stable pot. (V)
KNO_3		0.55	0.20
K_2SO_4	$1.4X10^{-5}$	0.50	0.00
KCl	$1.8X10^{-10}$	0.25	−0.20
KBr	$5.2X10^{-13}$	0.10	−0.40
KI	$8.3X10^{-17}$	−0.10	−0.60

CHAPTER 3

SURFACE ENHANCEMENT MECHANISMS

3.1 Raman Intensity and Enhancement Sources

When electromagnetic radiation interacts with matter the oscillating electronic field causes the matter to oscillate at the same frequency as the radiation. This response is expressed in terms of the induced dipole moment, which may be written

$$\mu = \alpha E + E \chi E \qquad (3\text{-}1)$$

where E ($=E_0 \cos\omega t$) is the electric field due to light of frequency ω and α is the polarizability, χ is the third order susceptibility. This expression may clearly be expanded to include higher order terms. Note that since the dipole moment is a vector quantity, as is E, α is then a second rank tensor and χ is a third rank tensor. Most normal and surface enhanced processes of interest depend only on the polarizability α.

The oscillations induced through the polarizability cause the matter to radiate light in all directions at the same frequency as the incident light. This process is known as Rayleigh scattering. We may understand this process more easily if we consider classically an electron of charge of -e bound elastically to an equilibrium position at which there is a charge +e. In the presence of an oscillating electric field the classical equation of motion is:

$$m d^2r / dt^2 + kr = -eE_0 \cos\omega t$$

Here r is the displacement of the electron from the origin and k is the force constant binding the electron. Letting $\omega_0 = (k/m)^{1/2}$, the steady state solution to this equation is:

$$r = \frac{-eE_0\cos\omega t}{m(\omega_0^2 - \omega^2)} = -\frac{\alpha}{e}E_0\cos\omega t$$

where we obtain an expression for the classical polarizability α by recognizing the classical expression for the dipole moment $\mu = er$. An electron with an acceleration a will radiate an amount of energy equal to $2e^2a^2/3c^3$ in one second where c is the speed of light. Since $a = d^2r/dt^2$ averaged over time we obtain a classical expression for the radiated energy to be $E_0^2\alpha^2\omega^4/3c^3$, we must then average over all directions in space, obtaining for the scattered intensity

$$I = 8\pi\omega^4 I_L \alpha^2 / 9c^4$$

in terms of the intensity of the exciting light

$$I_L = cE_0^2 / 8\pi \qquad (3\text{-}2)$$

In addition if the matter itself has natural oscillation frequencies ω_{IF} (such as the normal modes of a molecule, or phonon modes of a crystal) some light will also be radiated at the sum and difference frequencies $\omega \pm \omega_{IF}$. This process is known as Raman scattering. In order to conserve total energy in this process the matter is left either in a state of lower energy (for the sum, called the anti-Stokes spectrum) or higher energy (for the difference, called the Stokes spectrum). The total intensity of scattered radiation in photons per molecule per second, for a transition from the initial state I to the final state F is given by the expression:

$$I = 8\pi(\omega \pm \omega_{IF})^4 / 9c^4 I_L \alpha^2 \qquad (3\text{-}3)$$

or

$$I = (\omega \pm \omega_{IF})^4 / 9c^3 E_0^2 \alpha^2 \qquad (3\text{-}4)$$

For molecules adsorbed at a metal surface, one may consider two different enhancement sources:

1) an increase in the local field, E, experienced by the molecule adsorbed at the metal surface.

2) an enhancement of the effective polarizability, α_{eff}, of the metal/molecule system.

This distinction is convenient since field effects can be considered as strictly electromagnetic interactions of the dipole and the surface field, whereas chemisorption and other interactive effects can be modeled as modifications of the molecular polarizability. The enhancement of Raman scattering from both sources is a complex effect, and an extensive and diverse body of work has been developed to explain the phenomenon. In order to understand the respective contributions from various mechanisms to the observed enhancement in different systems, we review the theoretical works in three steps: 1) the mechanisms which require the mere presence of a conducting surface; 2) the electromagnetic enhancement by rough metal surface; 3) the chemisorption effect on the polarizability.

3.2 The Effect of a Smooth Metal Surface on Raman Scattering of Adsorbed Molecules

SERS was discovered at rough metal surfaces. However, in early studies of surface enhancement mechanisms theoretical models pertaining to smooth surfaces were invoked to help in understanding the SERS on a rough surface. The role of roughness cannot be completely understood without these studies. Besides, to

observe SERS at a smooth metal surface is very attractive from the technological point of view.

3.2.1 Image Field Effect (IFE)

In the simple image field effect (IFE) model, a point dipole is used to represent the oscillating dipole moment induced by the incident electromagnetic field. The metal surface boundary is assumed to be sharp and the metallic dielectric constant is assumed to be that of the bulk. The image dipole plus the original dipole can give rise to a very large electronic polarizability derivative relative to the molecular vibration coordinate (i.e., the Raman scattering cross section) when the molecule-metal separation distance is in the order of a few angstroms [25-29].

The relation for the dipole moment μ induced by the local field can be expressed by

$$\mu = \alpha_0(E_0 + E_{image}) \tag{3-5}$$

where α_0 is the polarizability of the free molecule, E_0 is the incident field and E_{image} is the field at the molecule which is caused by the image of the molecule in the adjacent metal. Since the entire system responds as a whole, the effective polarizability of the molecule in the presence of the surface can be defined as

$$\alpha_{eff} = \frac{\mu}{E_0} = \frac{\alpha_0}{1-\alpha_0 E_{image}/\mu} \tag{3-6}$$

As $\alpha_0 E_{image}/\mu \rightarrow 1$ the denominator of (3-6) goes to zero causing the effective polarizability to be greatly enhanced over the free molecule polarizability. This indicates that the singular nature of the Coulomb interaction of a point dipole with a metal surface may be an important source of the surface enhancement.

Since $E_{image} = \mu\gamma/4R^3$, where R is the separation of the induced dipole from the metal surface and $\gamma = (\epsilon_M - \epsilon_A)/(\epsilon_M + \epsilon_A)$ with ϵ_M and ϵ_A being the frequency dependent dielectric constants of the metal and adsorbate, respectively, α_{eff} becomes

$$\alpha_{eff} = \alpha_0 \left[1 - \frac{\gamma\alpha_0}{4R^3}\right]^{-1} \tag{3-7}$$

and its derivative relative to the molecular vibration coordinate Q will be

$$\frac{\partial\alpha_{eff}}{\partial Q} = \left[\frac{\alpha_{eff}(Q)}{\alpha_0(Q)}\right]^2 \frac{\partial\alpha_0(Q)}{\partial Q} \tag{3-8}$$

Since normal Raman intensity is proportional to $(\partial\alpha(Q)/\partial Q)^2$, the enhancement factor G will be in fourth order of α_{eff}/α_0 and thus twelfth order of 1/R,

$$G = \left|\frac{\alpha_{eff}}{\alpha_0}\right|^4 = \left|1 - \frac{\gamma\alpha_0}{4R^3}\right|^{-4} \tag{3-9}$$

From this formula an enhancement factor of 10^6 can be obtained at very small R However, the R^{-12}-dependence which predicts that changes in R of only a few hundredths of an angstrom will drastically affect the enhancement of the scattering is somewhat unphysical. Experimentally, image field theories have been shown to describe successfully the nonradiative decay of molecular electronic excitations for distances as close as 7 A to the surface [30]. At shorter distances, however, the approximations are less valid; image calculations of frequency shifts of molecular excitations for molecules on the surface have been shown to be seriously in error [31].

There have been several attempts to eliminate approximations in the simple

image model as sources of error in calculations. The point dipole is replaced by a sphere of finite radius [32] and by wavefunctions [33,34] and the sharp boundary is replaced by a continuous variation of electronic density across the interface [35-37]. The bulk k-independent dielectric constant $\epsilon(\omega)$ for the metal is replaced by a nonlocal k-dependent dielectric response function $\epsilon(k,\omega)$ to better account for the electron screening around the localized molecular adsorbate [32, 35-39]. Coupled eigenstates or coupled excitations of a physisorbed molecule and surface plasmons in the metal are treated quantum mechanically [39]. Finally, molecule-molecule interaction giving rise to a surface coverage dependence is also accounted for [28]. The main consequences of including these corrections in the image enhancement are a decrease in the maximum enhancement predicted at small distances. A decrease by a factor of 100 occurs for inclusion of nonlocal effects, and a further decrease of 10^2-10^3 occurs for inclusion of the effects of finite dipole size, resulting in an enhancement factor of less than 10^2.

3.2.2 Reflectivity Modulation (MP)

One of the models of this category proposed by McCall and Platzman [40] involves chemisorption at a metal surface. The Raman cross-section is enhanced by motion of charges from the metal into the molecule during nuclear vibrations. Motion of the adsorbate along the metal-adsorbate bond with an amplitude Δr produces a change in the metal susceptibility $\Delta\chi$ in a volume of metal involved in the charge transfer that is given by

$$\Delta\chi = \frac{\partial\chi}{\partial q}\frac{\partial q}{\partial r}\Delta r \qquad (3\text{-}10)$$

where q is the amount of charge transferred to the surface. The quantity $\partial\chi/\partial q$ is estimated from a free electron model of the metal where

$$\epsilon_M = 1 - \frac{\omega_p^2}{\omega^2} = 4\pi\chi + 1 \qquad (3\text{-}11)$$

Putting an extra electron per unit volume into the metal surface results in a change in the derivative of the susceptibility $\partial\chi/\partial q$ by $e^2/m\omega^2$. This results in a calculated Raman cross-section of

$$\frac{\partial\sigma}{\partial\Omega} = \frac{1}{3}\left|\frac{e^2}{mc^2}\right|^2\left|\frac{\partial q}{\partial r}\right|^2(\Delta r)^2 \qquad (3\text{-}12)$$

Estimating $\partial q/\partial r$ as 0.2 electron/A and Δr as 0.1 A, an enhancement of approximately 20 is predicted for a molecule in a chemisorbed system where there is vibrational displacement of the atom bound to the surface.

A similar reflectivity-modulation model was proposed by Otto [41] and developed by Maniv and Metiu [42]. It is based on the microscopic theory of reflection by a metal surface: reflection occurs when the metal absorbs a photon to create an electron-hole pair, which then recombine and emit a reflected photon. When a molecule is present on the surface the electron (or hole) can interact with the molecular ion cores through Coulombic forces and excite them vibrationally. The photon emitted by subsequent electron-hole pair recombination has the frequency $\omega - \omega_{IF}$ and is detected as a Raman photon. The model calculation is very complex and has used the jellium approximation with an infinite barrier 1.624 A from the jellium edge to described the metal surface. It was found that if the charge oscillating at the vibrational frequency is very close to the jellium edge (less than 0.5 A) a polarizability enhancement as large as 10^4 can be obtained. This large an enhancement, however, can only occur when the oscillation of nuclear charge can effectively induce electrons near the jellium edge to follow their oscillation.

3.2.3 Surface Plasmon Polaritons (SPP)

Differing from the above two models in which the enhancement results from the high effective polarizability, the SPP model gives rise to SERS through an enhanced local electromagnetic field. There are several ways of obtaining enhanced surface fields at the site of an adsorbed molecule. On a sinusoidally modulated metal surface with the product of incident wavevector and modulation height $k\xi << 1$, propagating surface electromagnetic waves can exist that an basically the well known surface plasmon polaritons (SPP, sometimes called just a surface plasmon) of a flat metal interface. This nonradiative mode can be excited by phase matching with the incident wavevector along the surface at appropriate optical frequencies. A solution of Maxwell's equations at the interface of a metal with dielectric constant $\epsilon_M(\omega)$ in contact with a medium of dielectric constant $\epsilon_A > 0$, gives the following equations for the electric fields of a plane wave at the interface:

$$E = E_0 e^{ikx - ikt} \times (1, 0, ik / (k^2 - \epsilon_A \omega^2 / c^2)^2) e^{-z(k^2 - \epsilon_A \omega^2 / c^2)} \qquad (3\text{-}12)$$

$$E = E_0 e^{ikx - ikt} \times (1, 0, ik / (k^2 - \epsilon_M \omega^2 / c^2)^2) e^{+z(k^2 - \epsilon_M \omega^2 / c^2)} \qquad (3\text{-}13)$$

Eq. (3-12) is for the region above the metal ($z > 0$) and Eq. (3-13) is for the region inside the metal ($z < 0$). The boundary condition for continuity of the z-component of the electric field at the interface gives the following relation:

$$\frac{\epsilon_M}{(k^2 - \epsilon_M \omega^2 / c^2)^{1/2}} = -\frac{\epsilon_A}{(k^2 - \epsilon_A \omega^2 / c^2)^{1/2}}$$

or

$$k^2 = \frac{\omega^2}{c^2} \frac{\epsilon_A \epsilon_M}{\epsilon_A + \epsilon_M} \qquad (3\text{-}14)$$

Such a surface wave is termed a SPP and Eq. (3-14) gives an explicit expression for

the magnitude of the wavevector of this mode as a function of frequency. SPP is confined to propagation along the interface and its electric field intensity rapidly decays into the metal and decays into the medium above the metal with a scale roughly equal to the wavelength of light [43].

When light is incident on the metal surface it couples only to excitation whose surface wavevector k is equal to the component of the wavevector of the incident light k_L that is parallel to the surface. The parallel component of the light is given by $k_L = (\omega/c)\sin\alpha$ where α is the angle of incidence of the light wave. The electromagnetic field on the interface becomes large when this resonance condition ($k=k_L$) is reached [44]. Consequently, when molecular adsorbates are situated on this interface, the molecules experience a much larger intensity resulting in an enhancement in Raman scattering. The enhancement is proportional to $1/\epsilon_2$, the imaginary part of the dielectric constant of the metal [45-48]; so that SPP can only be excited on metals with very little damping: i.e. Ag, Au, Cu, Al and alkali metals, etc.

Weber and Ford [49] have calculated the maximum enhancement in the local field intensity E^2 of the incident light at Ag, Au and Cu surfaces due to the excitation of SPP derived on the basis of energy conservation. They obtained maximum enhancements of 100-300 throughout the visible region for Ag and ca. 10-100 in the red for Cu and Au for perfect couplers. This is consistent with the enhancements of 25-80 observed in experiments on silver using both grating [50] and prism coupling [51].

For randomly rough surfaces, Jha *et al.* [52] excited their first order SPP theory for a single small amplitude grating to a sum of small amplitude Fourier

components of the roughness. Their calculated enhancements of up to 10^4 are an overestimate due to the neglect of the effect of roughness on the SPP themselves [49]. Weber and Ford [49] claim that due to absorption the enhancement for randomly rough surfaces is ca. 1 by energy conservation arguments. Arya *et al.* [53] have used a non-perturbative Green's function method to solve for enhancements of the incident field intensity on surfaces with Gaussian roughness and obtained enhancements of ca. 10^3 for Ag and ca. 10^2 for Au and Cu. Aravind and Metiu [54] have calculated the enhancement of the radiation from a dipole located over a randomly rough surface with rms amplitude $\delta = 30$ A and found an enhancement of ca. 10. To sum up, estimates of the total incident and scattered field enhancement by coupling to the considerably broadened SPP of a randomly rough Ag surface range from 1 to 10^4.

However, experiments have shown that much larger Raman signals can be detected when the metallic film is too thin (e. g. 5 nm) to sustain propagating SPP [55-57]. Such thin films rather exhibit islandlike structures when examined by SEM. The detected Raman effect was also found to be considerably larger after electrochemical oxidation and reduction had slightly roughened the surface of a thick smooth Ag film that had been optimized for SPP resonances [58,59]. These experiments have clearly illustrated that delocalized SPP alone do not give rise to SERS, though, in certain case, these propagating plasmons can give rise to an additional electromagnetic enhancement of 10-100 times, which may account for the incidence-angle dependence of SERS intensity observed in experiments [60-62].

3.2.4 Conclusion

After years of studies, it becomes clear that surface roughness both in submicroscopy and atomic scale is necessary for the giant enhancement. IFE, MP and SPP

mechanisms appear to be not practically important in most cases. Actually, the multichannel detection instrument has now enabled us to detect surface Raman scattering without enhancement. Compion and Mullins [63] have reported no enhancement of the Raman scattering cross section for pyridine at 120 K on the (100), (110) and (111) faces of silver in ultrahigh vacuum. The observed frequencies are essentially not shifted from those of liquid pyridine; intensity ratios are similar to the liquid; the signal intensity is linear in coverage from submonolayer to multilayer; the depolarization is low. These observations are in marked contrast to those associated with SERS. Although there have been many conflicting and irreproducible experimental results, general agreement on the following observations is now in order, which outline the extent of SERS and its characteristics as well as motivate the mechanistic discussion.

1. SERS occurs for a variety of molecules adsorbed on the surface of relatively few metals. The effect has been confirmed for silver, copper, gold and alkali metals that are highly reflective in the visible.

2. Surface roughness appears to be required. The major contribution can be either submicroscopic roughness (features of dimension 10-200 nm) or atomic scale roughness (steps, kinks, adatoms, or vacancies, for example), depending upon the system.

3. The enhancement may be remarkably long-ranged depending upon the surface topography. Appreciably enhanced scattering has been observed for molecules separated by tens of nanometers from the surface.

4. The excitation profile (dependence of the scattering intensity upon exciting frequency) deviates markedly from ω^4, displaying broad resonances in 450-700 nm region for Ag and 600-700 nm for Au and Cu.

5. The intensities of Raman bands generally fall off with increasing vibrational frequency.

6. The Raman bands are completely depolarized.

7. Molecules adsorbed in the first layer are often distinguishable from those adsorbed in adjacent layers by shifted vibrational frequencies, by the appearance of new bands and by larger enhancement factors.

8. Selection rules for Raman scattering are relaxed, resulting in the appearance of modes that are normally Raman inactive and even infrared inactive in the gas phase.

9. Surfaces that support SERS invariably display a weak continuum inelastic scattering, even in the absence of an adsorbed species.

10. Vibrational frequencies and excitation profiles are both functions of the applied potential in electrochemical experiments. The dependence of SERS intensity on excitation frequency and the applied potential is different for different vibrational modes.

Currently accepted mechanisms for SERS fall into two classes: electromagnetic and chemical. The former gives rise to SERS via enhanced local electromagnetic field and the latter contributes to SERS via an increased polarizability. The electromagnetic (EM) mechanism involves the excitation of conduction electron resonances at a rough metal surface by both the incident laser and the Raman oscillation. It addresses the interaction between the electromagnetic field of radiation and the conduction electrons at the metal surface. The effects of dielectric constants of the metal, the surface morphology, the separation between adsorbed molecules and metal surface enter into SERS via this field enhancement mechanism. The chemical mechanism, on the other hand, considers the interaction

between the adsorbed molecule and the metal surface. Theories of this class draw an analogy to resonance Raman scattering, involving adsorption induced charge transfer states as resonance intermediate states. These theories explain the roles of atomic structure of adsorbate-substrate and the applied potential in an electrochemical cell. Detailed discussions on these two kinds of theories will be made in the next two sections.

3.3 Roughness and Dipole Surface Plasmons (DSP)

The surface of SERS-active electrodes are very rough on a submicroscopic scale. The dissolution and redeposition of many layers of silver produce a surface that is covered with bumps of diameter 20-500 nm revealed by SEM photographs. These bumps can be approximated as spheres, hemisphere, and prolate spheroids [64,65]. In addition to rough electrodes, SERS has been observed for molecules adsorbed on colloids (resembling spheres) [66], on silver island films (resembling oblate spheroids) [67-69], and on silver ellipsoids prepared by evaporation on silicon posts[70]. These small structures all support electromagnetic resonances that are localized surface plasmons. The EM theory for localized plasmons has been developed for various isolated microstructures, such as, spherical particle [71], spheroids [72], prolate spheroids [73] and various other geometries [74].

3.3.1 Small Sphere Model

The simplest model used to calculate the EM enhancement by localized surface plasmon resonance is an isolated small sphere particle. If a spherical metal particle has a radius a which is small with respect to the wavelength of the laser light, i.e. $\lambda >> 20a$, the theoretical treatment of the electromagnetic enhancement factors is reduced to an electrostatic problem. The problem of finding the electric

field at R, where the molecule is located is treated by solving the Laplace equation, $\nabla\Phi = 0$ for the electrostatic potential, Φ, with the appropriate boundary conditions. The electric field is then found from the negative gradient of the electrostatic potential. The boundary conditions are

a) the potential at infinity $\Phi = -E_0 r\cos\theta$

b) the equality of the tangential electric field at r = a

$$-\frac{1}{a}\left|\frac{\partial\Phi_{in}}{\partial\theta}\right|_{r=a} = -\frac{1}{a}\left|\frac{\partial\Phi_{out}}{\partial\theta}\right|_{r=a}$$

c) the equality of the normal electric displacements at r = a

$$-\epsilon_M\left|\frac{\partial\Phi_{in}}{\partial r}\right|_{r=a} = -\epsilon_0\left|\frac{\partial\Phi_{out}}{\partial r}\right|_{r=a}$$

where ϵ_M and ϵ_0 are the dielectric constants of metal particle and its surroundings, respectively; Φ_{in} and Φ_{out} are the potentials inside and outside the metal sphere, respectively. The solutions are given in textbooks and for the potential outside the sphere it is found to be [75]

$$\Phi = -E_0 r\cos\theta + g\,(a^3/r^2)E_0\cos\theta \qquad (3\text{-}15)$$

with

$$g = \frac{\epsilon_M(\omega) - \epsilon_0}{\epsilon_M(\omega) + 2\epsilon_0} \qquad (3\text{-}16)$$

The first term in Eq (3-15) is the incident field and second term is from the field of an electric dipole located at the center of the sphere with polarizability ga^3 oriented in the direction of the incident field. Thus the local electric potential at position R is equivalent to that generated by the applied incident field and a reflected field produced by the metal sphere. The incident field polarizes the metal

sphere so that there develops surface charges of opposite sign on either side of the sphere which alternate with frequency ω as the electric field of the incident light changes sign. This mode is called a localized dipolar surface plasmon (DSP). In the long wavelength approximation, modes from higher multipoles need not to be considered. In contrast to the SPP's at a plane surface discussed previously, DSP's are radiative and can be excited by light incident on the sphere.

The average field in the radial direction, $\underline{E}_n$, at position R is found from the potential as given by Eq. (3-15) by taking the derivative with respect to r, i.e., $E_n = -\partial\Phi/\partial r$. The root mean square value comes from integration over the elements of solid angle $d\Omega = \sin\theta\, d\theta\, d\phi$ with limit of $\theta = 0$ to π and $\phi = 0$ to 2π.

$$\underline{E}_n = \langle E_n^2 \rangle^{1/2} = (1/3)^{1/2} E_0 [1 + 2g(a/R)^3] \tag{3-17}$$

Similarly, the tangential electric field components is obtained by the differentiation of Eq. (3-15) according to $E_t = -(1/r)(\partial\Phi/\partial\theta)$ and integration over the elements of solid angle,

$$\underline{E}_t = \langle E_t^2 \rangle^{1/2} = (2/3)^{1/2} E_0 [1 - g(a/R)^3] \tag{3-18}$$

Thus the electromagnetic (EM) enhancement factors can be defined,

$$L_n^2(\omega) = \frac{\underline{E}_n^2}{E_0^2} = \frac{1}{3}[1 + 2g(\frac{a}{R})^3]^2 \tag{3-19}$$

and

$$L_t^2(\omega) = \frac{2}{3}[1 - g(\frac{a}{R})^3]^2 \tag{3-20}$$

There is also a further EM enhancement effect to consider which is caused by the oscillating molecular dipole at position R inducing a dipole in the metal sphere.

Thus the metal sphere acts as an antenna for the near field of the oscillating molecular dipole and the emitted Raman radiation from the molecule at scattering frequency ω_s is then enhanced by the presence of the metal particle. The dipole of the entire system, the so called emission dipole of the system, molecule plus metal particle, includes the effect of both the enhanced electric field and the antenna effect. The antenna effect, to a good approximation, has the same form as $L^2(\omega)$; however, the frequency of light is now the Raman shifted scattering frequency, ω_s, giving a factor $L^2(\omega_s)$. This frequency is manifested in the dielectric function which becomes

$$g_s = \frac{\epsilon_M(\omega_s) - \epsilon_0}{\epsilon_M(\omega_s) + 2\epsilon_0} \tag{3-21}$$

The total EM enhancement at a spherical particle will be

$$G = L^2(\omega)\, L^2(\omega_s) \tag{3-22}$$

For a molecule adsorbed at a metal sphere (R=a) with its vibrational mode oriented normal to the surface, the average DPS enhancement is

$$G_{max} = L_n^2(\omega) L_n^2(\omega_s) = \frac{1}{9}(1 + 2g)^2(1 + 2g_s)^2 \tag{3-23}$$

From Eq. (3-16) it is apparent that when $\epsilon_M(\omega) = -2\epsilon_0$, the value of g becomes infinite which would maximize G. However, the dielectric functions are complex variables so that a zero in the denominator of g giving as infinite enhancement is, in fact, not possible since ϵ_M should be expressed as $\epsilon_M = \epsilon_1 + i\epsilon_2$. When resonance condition $\epsilon_1(\omega) = -2\epsilon_0$ is reached, the value of g is then $(-3\epsilon_0 + i\epsilon_2)/i\epsilon_2$ and for small ϵ_2, $|g^2| = |-3\epsilon_0/\epsilon_2|^2$. Thus the value of the imaginary coefficient of the dielectric function will determine the size of the enhancement at

resonance and the smaller ϵ_2 is, the larger will be the DSP enhancement. When the Raman shifted frequency ω_s is not too far from the exciting frequency ω_L, an approximation for the average DSP enhancement from a spherical metal particle is obtained when $g = g_s$ so that Eq. (3-23) becomes

$$\langle G \rangle_{max} \approx \frac{16}{9} g^4 \approx \frac{16}{9} \left| \frac{-3\epsilon_0}{\epsilon_2} \right|^4 = 144 \left| \frac{\epsilon_0}{\epsilon_2} \right|^4 \qquad (3\text{-}24)$$

Experimental values for ϵ_1 and ϵ_2 can be found for Ag, Au and other metals at optical frequencies [76,77]. For water at optical frequencies $\epsilon_0 = 1.77$ and thus the resonance condition is $\epsilon_1 = -2\epsilon_0 = -3.54$ which occurs at 382 nm for Ag. The imaginary component ϵ_2 is fairly constant and its approximately 0.3 in the 300-500 nm wavelength region for Ag according to the data of Johnson and Christy [76]. This value gives a $\langle G \rangle$ of 1.7×10^5 for Ag at 382 nm with the vibrational modes perpendicular to the surface. However, at 500 nm $\epsilon_1 = -10$ and letting $\langle G \rangle = 1/9(1 + 2g)^4$ give only 50 for the enhancement. Thus the DSP enhancement with a spherical metal particle cannot explain the 10^5-10^6 enhancement found with 488 nm and 514 nm laser excitation on Ag.

3.3.2 Small Spheroid Model

A more general EM model which may be a better representation of electrochemically pretreated SERS surfaces is to allow the metal particle to be a hemispherical protruding from a conducting plane. The spheroidal cross-section has a semi-major axis of length a and a semi-minor axis of length b with a focal point given by $f = (a^2 - b^2)^{1/2}$. The aspect ratio a/b defines the nature of the spheroid such that the particle becomes a sphere for $a/b = 1$, an oblate spheroid for $a/b < 1$, and a prolate spheroid for $a/b > 1$.

Solving the electrostatic boundary problem for a prolate metal spheroid, two major results are found: 1) Resonance frequency shifts to longer wavelength as a/b ratio becomes larger. For Ag in water, it moves from 388 nm (a/b=1) to 480 nm (a/b=2) to 580 nm (a/b=3); 2) As the aspect ratio a/b increases, the total enhancement at the tip increases, because the electric field at the tip is magnified. This is called the lightning rod effect. The maximum enhancement $G_M = 6.9\times10^8$ for a/b = 2 and $G_M = 6.0\times10^9$ for a/b = 3 Thus we see that the DSP resonance st a spheroidal metal particle and lightning rod effect can lead to extremely large enhancements for excitation throughout the visible region. Since in the actual experimental situation, there is a distribution of bump sizes and shapes on an electrochemically pretreated SERS metal surface and various possible molecular orientations, only a fraction of the sites will show the maximum enhancement. Furthermore, all molecules will not be located at the tip of the metal particles but will be distributed over the metal surface. These two effects greatly lower the net EM enhancement.

3.3.3 Large Particle and Electrodynamic Effects

Another important factor, the electrodynamic effect, tends to greatly lower the actually EM enhancement. SEM studies show that electrochemical pretreated SERS surfaces have particle sizes in the 20-500 nm range. For these large particles, a treatment based on the Rayleigh approximation ($\lambda/a >> 20$) is no longer valid. In this case an electrodynamic treatment based on Maxwell's equations rather than the electrostatic treatment using Laplaces equation is required. Such calculations have, indeed, been made using numerical solutions for the scattering problem [78,79]. In such a treatment, multipole terms higher than the dipole term become important. The result is that $L^2(\omega)$ decreases rapidly for radii above 10 nm [78].

Thus for an aspect ratio of a/b = 2 with a = 100 nm, the numerical calculations show a 980 fold decrease in $L^2(\omega)$ over that calculated from the electrostatic limit. This means an 8.1×10^3 decrease in the overall EM enhancement. Considering that surface averaging also decrease the tip enhancement by about a factor of around 17, we see that a maximum tip enhancement calculated within the Rayleigh approximation will be decreased by a factor of around 10^5 for the more exact treatment for large spheroids. Thus if all metal particles involved in the SERS scattering were spheroid with an aspect ratio of a/b = 2 and a semimajor axis of 100 nm, the total DSP enhancement would be around 1×10^3.

3.3.4 Summary

The first five experimental observations of SERS listed in section 3.2.4 can be qualitatively explained with the EM mechanism. SDP resonance occurs when $\mathrm{Re}\,\epsilon_M = -2\epsilon_0$ at either the laser frequency or the scattered frequency. Both excitation and emission can be resonant simultaneously if the vibrational frequency shift is not too large. Calculated resonant regions with the experimental value of ϵ_M explains well the excitation frequency region for observing SERS at Ag, Au and Cu surfaces. At resonance, the enhancement is proportional to $(\mathrm{Im}\,\epsilon_M)^{-4}$; this relationship explains why metals of high reflectivity (small $\mathrm{Im}\,\epsilon_M$) are better enhancers. The long-range nature of the enhancement is described by the $(a/R)^{12}$ dependence — molecules 5 nm away from a 25 nm radius particle still show 11% of the enhancement of the first layer (R=a=25 nm) molecules. The fall off in intensity of high frequency vibrations is also explained; the driving field and scattered field cannot simultaneously excite the particle resonance if they are of very different frequencies. Apparent discrepancies found in the reports from different laboratories and poor reproducibility in quantitative measurements of SERS can be

rationalized on the basis of different surface preparations, resulting in different size roughness features.

3.4 Chemical Adsorption and Charge Transfer Enhancement

3.4.1 Evidence for Chemical Enhancement

As mentioned before, electromagnetic mechanisms concern only metal-field interaction and an adsorbed molecule is simply assumed as a dipole located near the metal surface. However, the role of molecule-metal interaction in SERS is important as evidenced by molecule specificity of SERS. To say the least, widely variable SERS enhancements have been observed for molecules on surfaces having identical gas phase cross sections such as N_2 and CO on silver [80]. In general, molecules with a lone pair of electrons, such as a nitrogen heterocyclic, show stronger enhancement than others [81]. Chemisorption induced enhancement is thus proposed from these facts.

Further evidence for this additional mechanism beyond electromagnetic includes the first layer effect and the SERS active sites. Molecules adsorbed in the first layer are often distinguishable from those adsorbed in adjacent layers by shifted vibrational frequencies and different relative intensities. This indicates that a weak chemical bond is formed between the metal and the molecules in direct contact with the surface. In an electrochemical cell the physisorbed molecules can be easily removed by replacing the sample solution with the pure electrolyte solution after ORC, whereas the chemisorbed molecules remain at the surface. In our SERS study of the flavins (details are given in chapter 5), we found that 80-90% of the SERS intensity is retained after the replacement. This means that the observed SERS comes predominately from the first layer where the chemical enhancement

mechanism may act in addition to the EM enhancement. Other experiments further reveal that Ag adatoms or Ag clusters may have formed on a roughened Ag electrode, acting then as the so called SERS active sites [82,83]. The SERS of water which is always present in contact with the metal has only been observed in presence of co-adsorbed halides. It is strongly dependent on the bulk solution pH and the type of cation in the supporting electrolyte. Fleischmann *et al.* proposed that this form of water exists in a complex involving halides and Ag atoms [84]. Later investigators, while differing in detail, tend to agree with this concept. In order for SERS to be observed, water must exist at the active sites.

To study the role of active sites, several de-activation experiments have been conducted. The first experiment of this kind was performed by Wood and Klein [85] using pyridine on coldly evaporated Ag under UHV conditions. The observed SERS from such a system is irreversibly lost when the surface is annealed by warming to room temperature and then returning to the original temperature. Such experiments have been interpreted in terms of the loss of atomic scale defects during the annealing process [23]. However, the nature of the annealing is still an open question and the possibility exists that macroscopic restructuring took place [86]. An analogous process occurs for pyridine on electrodes which have been pre-treated by an ORC and then held at potentials negative to −1.2 V vs SCE. When the potential is brought back in a positive direction, short of that required for oxidation of the Ag, the scattering intensity is not re-established [87-90]. This phenomenon has been interpreted as resulting from the desorption of ligands from a SERS active silver adatom-ligand complex, allowing the adatoms to be incorporated into the metal lattice by surface diffusion and destroying SERS atomic scale active sites [89]. Thus electrode potential quenching is analogous to the temperature annealing.

Another possibility for quenching SERS active sites in the electrochemical environment is by underpotential deposition of metals such as Tl and Pb [91-93]. A very small underpotential coverage of deposited Tl, about 3%, leads to almost complete quenching of SERS from pyridine on Ag [91-93]. This quenching is irreversible since anodic stripping of Tl does not lead to restoration of the SERS signal. Underpotential deposition of Pb gives much weaker quenching and the quenching increases uniformly as the Pb coverage increases [91]. The Tl experimental results are interpreted in terms of the destruction of atomic scale active sites with a Ag atom being replaced by a Tl atom at a SERS active site [91,92]. Cu deposition on Ag leads to a shift in the pyridine spectrum typical of a Ag surface to that of a Cu surface at only 0.1 monolayer [93]. All these results indicate very high enhancements for molecules adsorbed at atomic scale active sites.

3.4.2 Charge Transfer Resonance Enhancement

It is well known that when a transition metal ion forms a complex with a ligand, a new charge transfer absorption band often occurs resulting in a color change. Very likely, a similar charge transfer transition takes place between an adsorbed molecule and the metal surface, especially when the molecule is chemisorbed at the active site. The polarizability is thus increased by the resonance effect. This basic idea is supported by the following experimental findings:

Creighton *et al.* [11] compared the optical absorption spectra of the Ag sols in presence and absence of pyridine. They found a new absorption band when pyridine was added. The SERS excitation profile of pyridine on Ag sol exhibits a maximum at approximately the same wavelength as that of the new absorption band.

In an electrochemical cell, Furtak *et al.* found that the voltage at which the

intensity reached a maximum (V_{max}) varied linearly with the excitation frequency (ω). A similar experimental results for pyridine/Ag [95,96] and CN^-/Ag [97] systems have also been reported by Otto and coworkers. At about the same time, Lombardi *et al.* in our laboratory showed this effect to exist for a variety of molecules [98]. They showed further that the molecules could be divided into two classes; those for which V_{max} had a positive slope with ω and those for which the slope was negative. This effect could be correlated to the electron withdrawing ability of the ground or excited electronic states of the molecules involved. These facts are taken as strong evidence for the existence of a metal-adsorbate charge transfer resonance mechanism for SERS.

A direct observation of low energy charge transfer bands for pyridine and pyrazine on silver was obtained by Demuth and Sanda [99] with high resolution electron energy loss spectroscopy. For pyridine, an affinity level has definitively been identified by inverse photoemission at 2.6 eV above the Fermi level by Otto *et al.* [100].

Based on these facts, a charge-transfer photon assisted SERS mechanism involving an electronic resonance between states of the metal and molecule was first suggested by a quantum mechanical treatment from our laboratory [101] and independently by other groups [102,103]. In a metal to molecule charge transfer, the process can be described [23] as a series of steps: 1) A metallic electron in an sp-conduction band absorbs a photon, the electron being promoted to the vacant sp-band above the Fermi level leaving a hole below the Fermi level in the filled sp-band; 2) the electron either tunnels to a temporary negative molecular complex or crosses over to an excited state of the molecule-metal system which is the charge transfer acceptor level of the chemisorbed molecule; 3) the electron returns

to the metal, recombines with the hole (assumed to be stationary) and in the process reradiates a Raman shifted photon; 4) the molecule is left in the excited vibrational state. If, in fact, there is any mixing of the zero order metal and the molecular wavefunctions, the momentum selection rule will have no meaning. Here then, the charge transfer process takes place between the surface adatom and the chemisorbed molecule, i.e., within the adatom-molecule complex. The charge transfer resonance energy is the difference between the adatom surface state level and the charge transfer acceptor level, both of which depend on the interaction energy H'.

A similar set of steps can be used to describe the molecule to metal charge transfer process [101]: 1) A ground state electron (in charge transfer donor level of the chemisorbed molecule) absorbs a photon and is vertically excited; 2) it either tunnels to a vacant level above the Fermi level of the metal forming a temporary positive molecule complex or crosses over to the lowest unoccupied level of the adatom surface state of the coupled molecule-adatom system; 3) the electron returns to the molecular ground electronic state and in the process reradiates a Raman shifted photon; 4) the chemisorbed molecule is left in an excited vibrational state. The charge transfer energy is the difference between the molecular ground state and the Fermi level in a weakly coupled molecule-metal system or the HOMO and the LUMO of a more strongly coupled molecule-adatom complex.

The broad background continuum which extends out to 4000 cm^{-1} can be explained by the charge transfer process in the adatom-molecule complex. If the hole, produced in the metal conduction band by metal to molecule charge transfer, loses a continuum of energy, subsequent electron-hole pair radiative recombination will lead to an inelastic continuum. On the other hand, loss of a continuum of

energy in the electron excited in the conduction band upon molecule to metal charge transfer also can lead to the inelastic continuum on subsequent radiative recombination with the unoccupied orbital on the molecule. It is also possible to envisage an enhanced inelastic continuum resulting from electron-hole pair excitations from adatoms by loss of a continuum of energy in either the hole or the excited electron. In this case the electron-hole excitation process does not have to involve the molecule.

In order to calculate the charge transfer enhancement factor, Persson [104] used a modified News-Anderson Hamiltonian from chemisorption theory, with the electron-photon interaction given by the dipole approximation and the vibronic interaction given by using the leading term in the Herzberg-Teller expansion. Assuming a Lorentzian functional form for the adsorbate density of states, he was able to generate the enhancement factor numerically with the Fermi level, the width of the adsorbate affinity level and the laser frequency as parameters. By his formula the estimated charge transfer enhancement factor for pyridine on Ag is ca. 30 which agrees with the experimental finding [105].

For a comprehensive theory there are, however, other pertinent experimental observations which must be explained. First, it is noted that overtones are observed only in a few cases although they are rather commonplace as predicted by the usual resonance Raman theory [106,107]. Second, the dependence of SERS intensity on excitation frequency and the applied potential is different for different vibrational modes. Third, experimental depolarization ratios in SERS all fall in the range of 0.6 to 0.75 even for totally symmetric vibrations. We answer these questions by a comprehensive development of the charge transfer theory of SERS to be presented in the next chapter followed by the application of the theory to the

determination of molecular orientation at the surface.

CHAPTER 4

CHARGE TRANSFER THEORY OF SERS

4.1 Introduction

In keeping with our experimental evidence and the basic concept of the charge transfer enhancement mechanism given in the previous chapter, we present here a theory of Raman intensities based on the Herzberg-Teller coupling mechanism as first formulated by Albrecht [106]. The theory will include both molecule-to-metal and metal-to-molecule charge transfer. A similar approach was taken by Adrian [108], who introduced vibronic coupling into the quantum mechanical expression for the polarizability limiting, however, his consideration only to the metal-to-molecule charge transfer. In so doing, two types of terms arise, one dependent only on Franck-Condon overlap integrals, and the second dependent on intensity borrowing from nearby allowed transitions. This latter term is called the Herzberg-Teller term. Adrian then claimed the latter term should be overwhelmed by the former and thereby ignored it. In considering the Franck-Condon term, Adrian obtained the correct dependence of V_{max} on the excitation frequency. However, we have found that his intensity vs voltage profile does not fit experimental profiles for reasonable values of the damping constants. His theory fails to explain adequately why overtones are rarely observed in SERS. Furthermore, the Franck-Condon term indicates that totally symmetric modes should be enhanced considerably more than nontotally symmetric modes. This is also contrary to what was observed. For example in piperidine [109] we observed that both a′ and a′′ modes are equally enhanced.

Metal-to-molecule charge transfer was also considered by Lippitsch [110]. He included vibronic coupling of the ground electronic state with states of the metal in an attempt to complement Adrian's theory. Unfortunately this theory falls short too in that it fails to predict any dependence of V_{max} on the excitation frequency. In the theory presented here the difficulties of both Adrian's and Lippitsch's theories are resolved. In the next section we apply the Herzberg-Teller conditions to a molecule-metal system without the approximation that the lowest energy gap is large, thereby maintaining the C term. In section 4.3 we apply the theory to the determination of molecular orientation at the surface.

4.2 Charge Transfer Theory of SERS

The intensity of a Raman transition is related to the polarizability tensor by the expression

$$I = (8\pi(\omega \pm \omega_{FI})^4 I_L / 9c^4)\sum |\alpha_{\sigma\rho}|^2, \tag{4-1}$$

where I_L is the incident laser intensity at frequency ω, while ω_{FI} is a molecular transition frequency between states I and F. ρ and σ each represents the three spatial directions x, y, z involved in the tensor. Using second-order perturbation theory it may be shown that

$$\alpha_{\sigma\rho} = \sum_{K \neq I,F} \left\{ \frac{\langle I|\mu_\sigma|K\rangle\langle K|\mu_\rho|F\rangle}{E_k - E_I - \hbar\omega} + \frac{\langle I|\mu_\rho|K\rangle\langle K|\mu_\sigma|F\rangle}{E_K - E_F + \hbar\omega} \right\}. \tag{4-2}$$

We consider states I, K, F to be vibronic in that they are assumed to be products of purely electronic functions with purely nuclear functions.

$$\Psi_I(q,Q) = \Theta_I(q,Q)\Phi_i^I(Q), \tag{4-3}$$

where $\Phi_i^I(Q)$ is the vibration of state I with i quanta of the normal mode Q excited. $\Theta_i(q,Q)$ is the electronic part of the wave function for the state I which depends on the electronic coordinates q and parameterically on the nuclear coordinates Q. In the following it will be more convenient to use for Eq. (4-3) the shorthand notation

$$|I> = |I_e>|i>, \tag{4-4}$$

where the subscript e indicates a purely electronic function. In this notation $|K> = |K_e>|k>$ represents the vibronic excited states and the final Raman transition is written $|F> = |I_e>|f>$. Following Tang and Albrecht [107] we consider the electronic transition moment can be written

$$\begin{aligned} <I|\mu|K> &= <i|M_{IK}(Q)|K>, \\ M_{IK}(Q) &= <I_e|\mu|K_e> \end{aligned} \tag{4-5}$$

which is assumed through Eq. (4-3) to be weakly dependent on the nuclear coordinates. It is the heart of Herzberg-Teller theory that even small vibrations may cause mixing of zero order Born-Oppenheimer states, allowing us to write

$$|K_e> = |K_e,0> + \sum\lambda_{KM}(Q)|M_e,0>, \tag{4-6}$$

$$\begin{aligned} \lambda_{KM}(Q) &= h_{KM}(Q)/(E_K^0 - E_M^0), \\ h_{KM}(Q) &= <K_e,0|\partial H'/\partial Q|M_e,0>, \end{aligned} \tag{4-7}$$

where zeros refer to zero order Born-Oppenheimer states. The sum over M runs over all the excited states. $h_{KM}(Q)$ are coupling matrix elements for terms in the Hamiltonian H′ normally neglected in the Born-Oppenheimer approximation. They represent the degree to which a particular vibration Q can mix state M with state K. Similarly for the ground state

$$|I_e> = |I_e,0> + \sum \lambda_{IM}(Q)\,|M_e,0>, \qquad (4\text{-}8)$$
$$\lambda_{IM}(Q) = h_{IM}(Q)/(E_I^0 - E_M^0).$$

Substituting into Eq. (4-2) we obtain

$$\alpha_{\sigma\rho} = A + B + C, \qquad (4\text{-}9)$$

$$A = \sum_{K\neq I}\sum_{k}\left|\frac{M_{KI}^{\sigma}(Q_0)M_{KI}^{\rho}(Q_0)}{\hbar(\omega_{KI} - \omega)} + \frac{M_{KI}^{\rho}(Q_0)M_{KI}^{\sigma}(Q_0)}{\hbar(\omega_{KI} + \omega)}\right|<i|k><k|f>, \qquad (4\text{-}10)$$

$$B = \sum_{k\neq I}\sum_{k}\sum_{M\neq K}\left|\frac{M_{IK}^{\sigma}h_{KM}M_{MI}^{\rho}}{\hbar(\omega_{KI} - \omega)} + \frac{M_{IK}^{\rho}h_{KM}M_{MI}^{\sigma}}{\hbar(\omega_{KI} + \omega)}\right|\frac{<i|k><k|Q|f>}{\hbar\omega_{MK}}$$

$$+ \left|\frac{M_{IM}^{\sigma}h_{MK}M_{KI}^{\rho}}{\hbar(\omega_{KI} - \omega)} + \frac{M_{IM}^{\rho}h_{MK}M_{KI}^{\sigma}}{\hbar(\omega_{KI} + \omega)}\right|\frac{<i|Q|k><k|f>}{\hbar\omega_{MK}}, \qquad (4\text{-}11)$$

$$C = \sum_{K\neq I}\sum_{k}\sum_{M\neq I}\left|\frac{h_{IM}M_{MK}^{\sigma}M_{KI}^{\rho}}{\hbar(\omega_{KI} - \omega)} + \frac{h_{IM}M_{MK}^{\rho}M_{KI}^{\sigma}}{\hbar(\omega_{KI} + \omega)}\right|\frac{<i|k><k|Q|f>}{\hbar\omega_{IM}}$$

$$+ \left|\frac{M_{IK}^{\sigma}M_{KM}^{\rho}h_{MI}}{\hbar(\omega_{KI} - \omega)} + \frac{M_{IK}^{\rho}M_{KM}^{\sigma}h_{MI}}{\hbar(\omega_{KI} + \omega)}\right|\frac{<i|Q|k><k|f>}{\hbar\omega_{IM}}. \qquad (4\text{-}12)$$

This is the expression derived by Tang and Albrecht [107]. At this point they observed that in most molecular systems the energy gap between the ground state and all the other states is much larger than the gaps between excited states, or that $|\omega_{IM}| >> |\omega_{KM}|$. On this basis they ignored the term C. However, we are considering a molecule-metal system in which this cannot be done. We assume that states $|M>$ may lie between $|I>$ and $|K>$ and therefore C cannot be discarded (see Fig. 4-1(a)). We assume further that there is at least one state K to which there is an allowed transition from the ground state (i.e., $M_{IK}\neq 0$). Note that in the limit of large distance between molecule and metal we should expect that the matrix elements M_{IM} and M_{MK} representing molecule-to-metal and metal-to-molecule charge

Figure 4-1

(a) Energy level scheme for molecule-metal system. The (discrete) molecular levels are I and K, between which a transition is assumed to be allowed. The (continuous) metal levels of the conduction band of the metal are shown on the left. The conduction band ranges between ω_A and ω_B and is assumed to have a constant density of states ρ_o. The filled levels range up to ω_F, the Fermi level, and are depicted by lines, while the unfilled levels are depicted by dots. Applied potential is represented by V and ω_{F_o} is the Fermi level at zero potential.

(b) The scheme for molecule-to-metal charge transfer transitions between the ground molecular state and unfilled levels of the metal. The transition, M_{IM}, is assumed to be allowed.

(c) The scheme for metal-to-molecule charge transfer transitions between filled levels of the metal and the excited molecular state. The transition, M_{MK}, is assumed to be allowed.

(d) The scheme for molecule-to-metal charge transfer transitions which borrow intensity from the allowed transition, M_{IK}, by means of vibronic coupling between metal levels and the excited molecular level through the matrix element, h_{MK}.

(e) The scheme for metal-to-molecule charge transfer transitions which borrow intensity from the allowed transition, M_{IK}, by means of vibonic coupling between metal levels and the ground molecular state through the matrix element, h_{IM}.

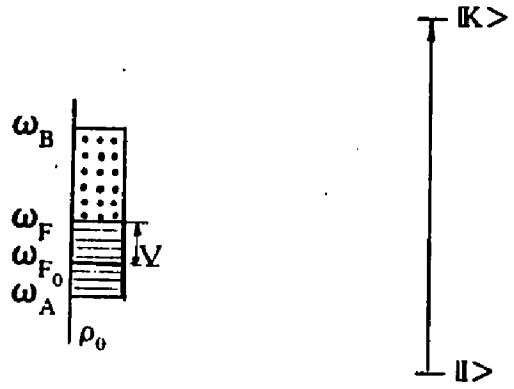

(a) separated metal-molecule system

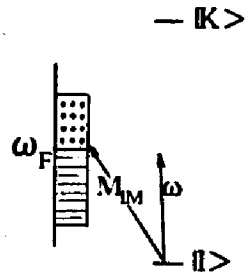

(b) A_f term

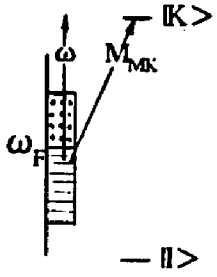

(c) A_k term

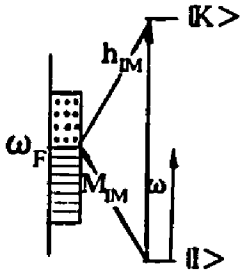

(d) B term

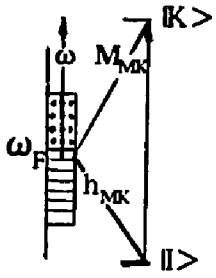

(e) C term

transfer transitions to be zero. However, when the molecule forms a weak chemical bond with the surface, we can no longer treat the molecule and metal as separate systems, and there is no reason to expect them to be zero. Furthermore the matrix elements h_{IM} and h_{KM} representing the vibronic mixing of metal states with ground and excited states are assumed to be nonzero in the combined system.

We now consider the situation in which the frequency of the exciting light is far from any molecular resonance ($\omega << \omega_{IK}$). Then in each of the Eqs. (4-10)-(4-12) we may remove the frequency dependent terms from the summation over all vibrational states k. Utilizing the closure relation $\Sigma|k><k| = 1$ we see that in Eq. (4-10) $\Sigma <i|k><k|f> = <i|f>$ vanishes in the harmonic oscillator approximation unless i = f. Thus far from a molecular resonance the term A contributes only to the Rayleigh line. If alternatively we consider in term A those states in which either K or I is actually a metal state, we might expect resonant contributions to the intensity, and we cannot carry out the sum over vibrational states if the laser width is less than molecular vibrational spacings. In the latter case a single vibration will dominate the sum. We have for $|K> = |M>$:

$$A_f = (2/\hbar)\sum_M M_{Mf}^{\sigma} M_{Mf}^{\rho} <i|k><k|f> \frac{\omega_{MI} + \omega_f}{(\omega_{MI} + \omega_f)^2 - \omega^2} \qquad (4\text{-}13)$$

while for $|I> = |M>$ we obtain

$$A_k = (2/\hbar)\sum_M M_{KM}^{\sigma} M_{KM}^{\rho} <i|k><k|f> \frac{\omega_{KM} + \omega_k}{(\omega_{KM} + \omega_k)^2 - \omega^2}, \qquad (4\text{-}14)$$

where ω_k and ω_f are the frequencies of a particular excited and ground state vibration, respectively. Term A_f represents resonant molecule-to-metal charge transfer from the molecular ground state to one of the unfilled metal levels M, as

illustrated in Fig. 4-1(b), while A_k represents resonant metal-to-molecule charge transfer from a filled metal state M to an excited state K, which is illustrated in Fig. 4-1(c). The sum over vibrational state k has been removed.

In considering both B and C we confine ourselves to cases where ω is far from any molecular resonance. We may then utilize $\Sigma \langle i|k\rangle\langle k|Q|f\rangle = \langle i|Q|f\rangle$. Following Tang and Albrecht [107] we recognize that in the sum over states M there are terms in which M and K (for B) or M and I (for C) are interchanged. We may combine terms pairwise to obtain

$$B = -(2/\hbar^2) \sum_{K \neq I,M} \sum_{<K} (M_{KI}^{\sigma} M_{MI}^{\rho} + M_{KI}^{\rho} M_{MI}^{\sigma}) \frac{(\omega_{KI}\,\omega_{MI} + \omega^2) h_{KM} \langle i|Q|f\rangle}{(\omega_{KI}^2 - \omega^2)(\omega_{MI}^2 - \omega^2)}, \tag{4-15}$$

$$C = -(2/\hbar^2) \sum_{K \neq I,M} \sum_{>I} (M_{MK}^{\sigma} M_{KI}^{\rho} + M_{MK}^{\rho} M_{KI}^{\sigma}) \frac{(\omega_{KI}\,\omega_{KM} + \omega^2) h_{IM} \langle i|Q|f\rangle}{(\omega_{KI}^2 - \omega^2)(\omega_{KM}^2 - \omega^2)}. \tag{4-16}$$

We may now interpret these results in terms of SERS. Term B represents the molecule-to-metal charge transfer from the molecular ground state to one of the unfilled metal levels M. This transition obtains its intensity via M_{MI} through intensity borrowing from the (assumed) allowed transition $I \rightarrow K$. This is illustrated in Fig. 4-1(d). The borrowing mechanism is vibronic coupling through h_{KM} which represents coupling of the metal to excited molecular states through some vibrational mode. The requirement that this term be nonvanishing imposes some symmetry restrictions on the vibrations which may then be responsible for the mixing. Note that the enhancement comes through the resonance denominator $\omega_{MI}^2 - \omega^2$.

Term C represents the metal-to-molecule charge transfer from one of the filled metal levels M to the excited state K. This transition obtains its intensity via M_{MK} through intensity borrowing from the allowed $I \rightarrow K$ transition. h_{IM} represents vibronic coupling of the metal to the ground molecular level through some vibrational mode. This is illustrated in Fig. 4-1(e). Note that the enhancement comes through the resonance denominator $\omega_{KM}^2 - \omega^2$.

The selection rules for each term can now be deduced from these resulting formulas. Equations (4-15) and (4-16) indicate that in order for B or C to be nonvanishing $\langle i|Q|f\rangle$ must be nonzero. This leads to the usual selection rule that $f = i \pm 1$ in the harmonic oscillator approximation. It is further required for B that neither h_{KM} nor appropriate components of M_{KI} and M_{MK} vanish. For C we require neither h_{IM} nor components of M_{MK} and M_{KI} vanish. For B assuming a totally symmetric ground state, these observations imply that the symmetry species Γ_M and Γ_K of these electronic states must each correspond to Γ_ρ, the species of at least one translation. At the same time, the direct product $\Gamma_K\Gamma_Q\Gamma_M$ must contain the totally symmetric representation to prevent h_{KM} from vanishing. By Γ_Q we mean the irreducible representation for which $(\partial H'/\partial Q)$ is a basis which is the same as that for Q. Thus if $\Gamma_K = \Gamma_\rho$ and $\Gamma_M = \Gamma_{\rho'}$ it is required that Γ_Q must correspond to at least one of the species contained in $\Gamma_\rho\Gamma_{\rho'}$ which are the normal selection rules for the Raman effect. A similar analysis for the term C leads to an identical conclusion.

In contrast, Equations (4-13) and (4-14) show that $f = i \pm 1$ is not required for A_k and A_f to be nonzero, because the overlap integrals $\langle i|k\rangle$ and $\langle k|f\rangle$ involve the vibrational wavefunctions of two different electronic states. However, in order that both M_{MI}^{σ} and M_{MI}^{ρ} (i.e. $\langle M\mu_\sigma|I\rangle$ and $\langle M\mu_\rho|I\rangle$) in A_f are nonzero at the

same time, $\Gamma_M\Gamma_I$ necessarily belongs to the same irreducible representation of σ and ρ simultaneously. Since none of the nontotally symmetric mode $\alpha_{\sigma\rho}$ meets this requirement, the enhancement through A_f (A_k also) is possible only for totally symmetric vibrational modes.

We can see now that although all four terms have a resonance denominator in their formulas they follow different selection rules. Two Herzberg-Teller (HT) terms B and C have the same selection rules as the normal Raman scattering. All vibrational (both totally and nontotally symmetric) modes can be resonance enhanced through intensity borrowing. On the other hand, the two Franck-Condon (FC) terms, A_f and A_k, are like usual resonance Raman. Overtones are allowed but nontotally symmetric vibrations are forbidden. Only one report [111] so far clearly shows the appearance of overtones and combination bands of some totally symmetric vibrational modes from phenazine adsorbed on a silver electrode. Another report [112] gave only very weak overtones. Weak overtones in SERS can be explained by the fact that both FC and HT terms can contribute to the fundamental bands of totally symmetric vibrational modes, but only FC term contributes to overtones because in the harmonic oscillator approximation we expect no overtones to be allowed in HT terms.

We may now find the resonance conditions for each term from the resonance denominators in the formulas (4-13) to (4-16). The sum over metal states can be carried out by recognizing that the metal states are so closely spaced that the sum may be replaced by an integral over the energy. For molecule-to-metal charge transfer, it runs from the Fermi level ω_F to the up-bound of the conduction band ω_B, while for metal-to-molecule charge transfer, it runs from the low-bound ω_A to the Fermi level ω_F [113]. Then we find that the resonance occurs at

$$\omega = \omega_{FI} + \omega_f \quad \text{for } A_f , \tag{4-17}$$

$$\omega = \omega_{FI} \quad \text{for } B , \tag{4-18}$$

$$\omega = \omega_{KF} + \omega_k \quad \text{for } A_k , \tag{4-19}$$

$$\omega = \omega_{KF} \quad \text{for } C. \tag{4-20}$$

Since

$$\omega_{FI} = \omega_{F_0 I} + V$$

$$\omega_{KF} = \omega_{KI} - \omega_{F_0 I} - V$$

as illustrated in Fig. 4-1(a), where V is the applied potential and $\omega_{F_0 I}$ is the energy difference between the Fermi level of zero voltage and the ground state of the molecule, we can rewrite Eqs. (4-17)-(4-20) to obtain the voltage maximum of intensity:

$$V_{max} = -\omega_{F_0 I} - \omega_f + \omega \quad \text{for } A_f \tag{4-21}$$

$$V_{max} = -\omega_{F_0 I} + \omega \quad \text{for } B \tag{4-22}$$

$$V_{max} = \omega_{KI} - \omega_{F_0 I} + \omega_k - \omega \quad \text{for } A_k \tag{4-23}$$

$$V_{max} = \omega_{KI} - \omega_{F_0 I} - \omega \quad \text{for } C \tag{4-24}$$

Most generally we expect either molecule-to-metal charge transfer in which A_f and B must be considered or metal-to-molecule charge transfer in which A_k and C must be considered. It is unlikely that charge transfer in both directions would occur simultaneously. In either case notice that only totally symmetric modes can be resonance enhanced through the FC term. We then regard totally symmetric vibrations as having possible contributions from both FC and HT terms and nontotally symmetric vibrations have contributions only from HT terms. This viewpoint has an added feature of being able to explain why the voltage maximum of intensity, V_{max}, is often slightly different for totally symmetric vibrations than for nontotally symmetric vibrations [114]. Note that in Eqs. (4-21) and (4-22), the FC term gives a V_{max} more negative than that from HT term by ca. 0.2

eV, since ω_k, the vibrational frequency, is usually in this order of magnitude. In Eqs. (4-23) and (4-24), the V_{max} from FC term is more positive than that from HT term by the same amount. We predict that for molecule-to-metal charge transfer totally symmetric modes should display V_{max} at a voltage more negative than non-totally symmetric modes. The reverse should be true for metal-to-molecule charge transfer. This is just what we have observed [114]. In piperidine (molecule-to-metal charge transfer), the A′ modes peak at −0.8 V while the A″ modes peak near −0.5 V, and in pyridine (metal-to-molecule charge transfer), the a_1 modes peak near −0.6 V while the b_1 modes peak at −0.9 V.

4.3 Overall Intensity Equations of SERS and Molecular Orientation

Observed SERS usually result from both electromagnetic enhancement of a rough metal surface and the charge transfer resonance enhancement upon chemisorption. Replacing E_o^2 with E_{sur}^2 ($=E_0^2L^2(\omega)L^2(\omega_s)$) and replacing α^2 with $\alpha_{CT}^2(\omega,V)$ in the intensity Eq. (3-3) for conventional Raman scattering, we obtain

$$I_{SERS} = \frac{(\omega \pm \omega_{IF})^4}{9c^3} E_0^2 L^2(\omega) L^2(\omega_s) \alpha_{CT}^2(\omega,V)$$

or in terms of the intensity of the exciting laser light,

$$I_{SERS} = \frac{8\pi(\omega \pm \omega_{IF})^4}{9c^4} I_L L^2(\omega) L^2(\omega_s) \alpha_{CT}^2(\omega,V) \qquad (4\text{-}25)$$

Note now that the normal and tangential enhancement components of the local field at a small metal sphere are different. The formulas have been given in Eqs. (3-19) and (3-20). For simplicity, let R = a and thus

$$L_n^2(\omega) = \frac{1}{3}[1 + 2g(\omega)]^2 \qquad (4\text{-}26)$$

$$L_t^2(\omega) = \frac{2}{3}[1 - g(\omega)]^2 \qquad (4\text{-}27)$$

where $g(\omega)$ is a function of light frequency (Eq. 3-16). On plasmon resonance (near UV, $g >> 1$) the enhancement factors in these two directions are thus in the ratio 2:1. Far off resonance (in IR, $g \simeq 1$) the tangential field is zero. In visible region the enhancement factor at normal direction is always larger than that at tangential direction and L_t^2 to L_n^2 ratio decreases with increasing excitation wavelength. Based on these arguments surface selection rules for SERS have been given by Creighton [115] and Moskovits *et al.*[116] and were used to deduce molecular orientations at the surface. The pyridine molecules were determined to be lying down flat on the Ag electrode at −0.5 V from the fact that the b_2 modes, which correspond with $L_t^2 L_t^2$ in the flat configuration, are uniformly the least enhanced [115]. The phthalazine molecules were found standing up on the silver colloidal surface by comparing the intensity ratios of a_2 to b_1 (or b_2 to b_1) modes with 488- and 647.1-nm excitations [116]. However, questions could be raised on the basis of these works concerning whether the charge transfer enhancement acts differently on vibrations of different symmetry classes. These questions include what the differences are and if the charge transfer effect can be separated out and will be discussed in terms of the formulas obtained in the previous section.

Since new electron transition dipole moments between the metal and the molecule are involved in α_{CT}, molecular vibrations are generally enhanced differently depending upon the directions of the vibration with respect to the transition dipole moment or the mixing matrix element. Relative enhancement factors range from 1 to 10.5 were found for pyridine on a Ag electrode [115]. Therefore, the rule that vibrations normal to the surface are enhanced more than those at tangential direction may not be always true when taking into account the charge

transfer effect. The method used by Moskovits *et al.* [116] can, however, avoid the problem as discussed in the following.

At a metal surface vibrational modes can be classified into three groups depending upon different correspondence with the EM enhancement factors:

$$\begin{aligned} &\alpha_{zz}: && L_n^2 L_n^2 = \frac{1}{9}(1+2g(\omega))^4 \\ &\alpha_{xz}, \alpha_{yz}: && L_n^2 L_t^2 = \frac{1}{9}(1+2g(\omega))^2(1-g(\omega))^2 \\ &\alpha_{xx}, \alpha_{yy}, \alpha_{xy}: && L_t^2 L_t^2 = \frac{4}{9}(1-g(\omega))^4 \end{aligned} \tag{4-28}$$

where x, y, z are surface fixed coordinates with z normal to the surface and $g(\omega_s)$ is replaced with $g(\omega)$ for simplicity.

For a molecule with C_{2v} symmetry like phthalazine or pyridine, the irreducible representations are

$$\begin{aligned} &a_1: && X^2, Y^2, Z^2 \\ &a_2: && XY \\ &b_1: && XZ \\ &b_2: && YZ \end{aligned} \tag{4-29}$$

for the molecule fixed coordinates. If the molecule is standing up, then in terms of surface fixed coordinates $X \rightarrow x$, $Y \rightarrow y$, and $Z \rightarrow z$; however if the molecule is lying down, then $X \rightarrow z$, $Y \rightarrow y$, and $Z \rightarrow x$ as illustrated in Fig. 4-2. According to the relationship in Eq. (4-28) and Tab. 4-1, the ratio of band intensities of b_1 symmetry to that of b_2 symmetry for the molecule lying down should depend on the enhancement factors roughly as L_n^2/L_t^2. On the other hand if the molecule is standing up, these modes couple into the same enhancement factor products, the band ratios should be independent of the enhancement factors.

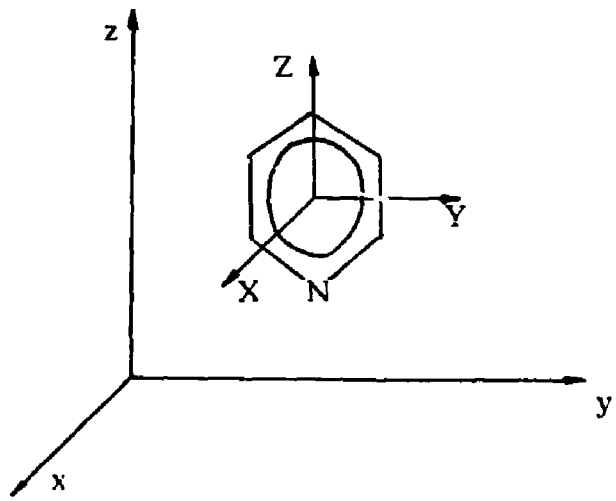

(a) standing-up

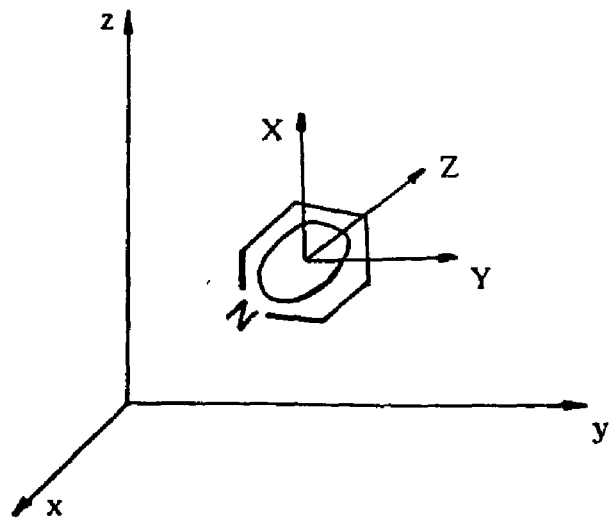

(b) lying-down

Figure 4-2. Possible orientations of pyridine on a metal surface.

Table 4-1

EM Enhancement Factors as a Function of Surface Orientation for C_{2v} Symmetry

C_{2v}	$\alpha_{\sigma\rho}$	Standing-up	Lying-down
a_1	XX	$L_t^2L_t^2$	$L_n^2L_n^2$
	YZ	$L_t^2L_t^2$	$L_n^2L_n^2$
	ZZ	$L_n^2L_n^2$	$L_t^2L_t^2$
a_2	XY	$L_t^2L_t^2$	$L_n^2L_t^2$
b_1	XZ	$L_n^2L_t^2$	$L_n^2L_t^2$
b_2	YZ	$L_n^2L_t^2$	$L_t^2L_t^2$
$\frac{(a_2/b_1)_{blue}}{(a_2/b_1)_{red}}$		>1	$=1$
$\frac{(b_2/b_1)_{blue}}{(b_2/b_1)_{red}}$		$=1$	>1

Now let us concern the charge transfer effect. The ratio of two nontotally symmetric modes for pyridine (metal-to-molecule charge transfer) can deduced from Eq. (4-16)

$$\left|\frac{\alpha_{\sigma\rho}^{i,f}}{\alpha_{\sigma\rho}^{i,f'}}\right|^2 = \left|\frac{(M_{KI}^{\sigma} M_{MI}^{\rho} + M_{KI}^{\rho} M_{MI}^{\sigma}) h_{KM} \langle i | Q | f \rangle}{M_{KI}^{\sigma} M_{MI}^{\rho} + M_{KI}^{\rho} M_{MI}^{\sigma} h'_{KM} \langle i' | Q | f' \rangle}\right|^2 \qquad (4\text{-}30)$$

Note that the frequency and the potential dependence of the B term is independent of vibrational modes and is thus canceled out in the ratio. This allows one to make use of the different frequency dependences of the normal and tangential EM enhancement factors to determine molecular orientations. Combining EM and CT factors, observed SERS intensity ratio for b_2 and b_1 bands is determined by

$$\frac{I_{b_2}}{I_{b_1}} = \begin{cases} K_{ct} & \text{if standing up} \\ K_{ct}\dfrac{2(1-g(\omega))^2}{(1+2g(\omega))^2} & \text{if lying down} \end{cases} \qquad (4\text{-}31)$$

where K_{ct} is a constant determined by Eq. (4-30) and may differ for the two configurations. Since $g(\omega)$ is a function of frequency, the intensity ratio for the lying down configuration is expected varying with the excitation frequency. To blue of the localized surface plasmon peak, the ratio progressively increases but to the red of the peak it gradually decreases. Therefore, we have:

$$\frac{(I_{b_2}/I_{b_1})_{blue}}{(I_{b_2}/I_{b_1})_{red}} \begin{cases} = 1 & \text{if standing up} \\ > 1 & \text{if lying down} \end{cases} \qquad (4\text{-}32)$$

A similar conclusion can be drawn for a_2/b_1 ratios as listed in Tab. 4-1. Based on the above arguments, we conclude that the CT effect can be separated out by measuring the frequency dependence of intensity ratios for any two nontotally

symmetric vibrational bands and the molecular orientation can be deduced from this measurement. Since the ratio in Eq. (4-32) is also independent of the applied potential, the change in orientation upon the potential, if any, can also be determined.

As a test of the above considerations we have made intensity ratio measurements for pyridine at a pretreated Ag electrode as a function of potential. The ORC pretreatments were carried out in dark with three sweeps from −0.4 V to 0.3 V and then back to −0.4 V vs SCE at 50 mV/s in the 0.05 M pyridine and 0.1 M KCl solution. The bands used for the measurements are 383 $cm^{-1}(a_2)$, 414 cm^{-1} (b_1), 879 $cm^{-1}(a_2)$, 944 $cm^{-1}(b_1)$, 1155 $cm^{-1}(b_2)$ and 1444 $cm^{-1}(b_2)$ as shown in Fig. 4-3. The band intensity is measured by the peak height. It was found that the two $(a_2/b_1)_{488}/(a_2/b_1)_{647}$ intensity ratios are close to unity and two $(b_2/b_1)_{488}/(b_2/b_1)_{647}$ intensity ratios are greater than 1 at −0.6 V vs SCE as listed in Tab. 4-2. This indicates that the pyridine molecule is lying down on the Ag electrode surface in agreement with the result of Creighton [115] at − 0.5 V vs SCE. The potential dependence of these ratios were obtained from −0.4 to 1.0 V vs SCE. As can be seen in Fig. 4-4, the a_2/b_2 ratios are greater than 1.0 at the potentials more negative than −0.6 V, while the b_2/b_1 ratios decreases to unity when potentials are more negative than −0.6 V. This indicates a change in molecular orientation from lying-down to standing-up occurs at ca. −0.7 V vs SCE. However, the b_2/b_1 ratio at −0.4 V is close to unity giving a contrary conclusion to what was deduced from the a_2/b_1 ratio. It is possible that the approximation made in our CT theory that the electron transition dipole moment between molecule and metal is independent of the potential is not valid in some cases. It is also possible that there is no preferred orientation at −0.4 V. In any case the method should be used with caution.

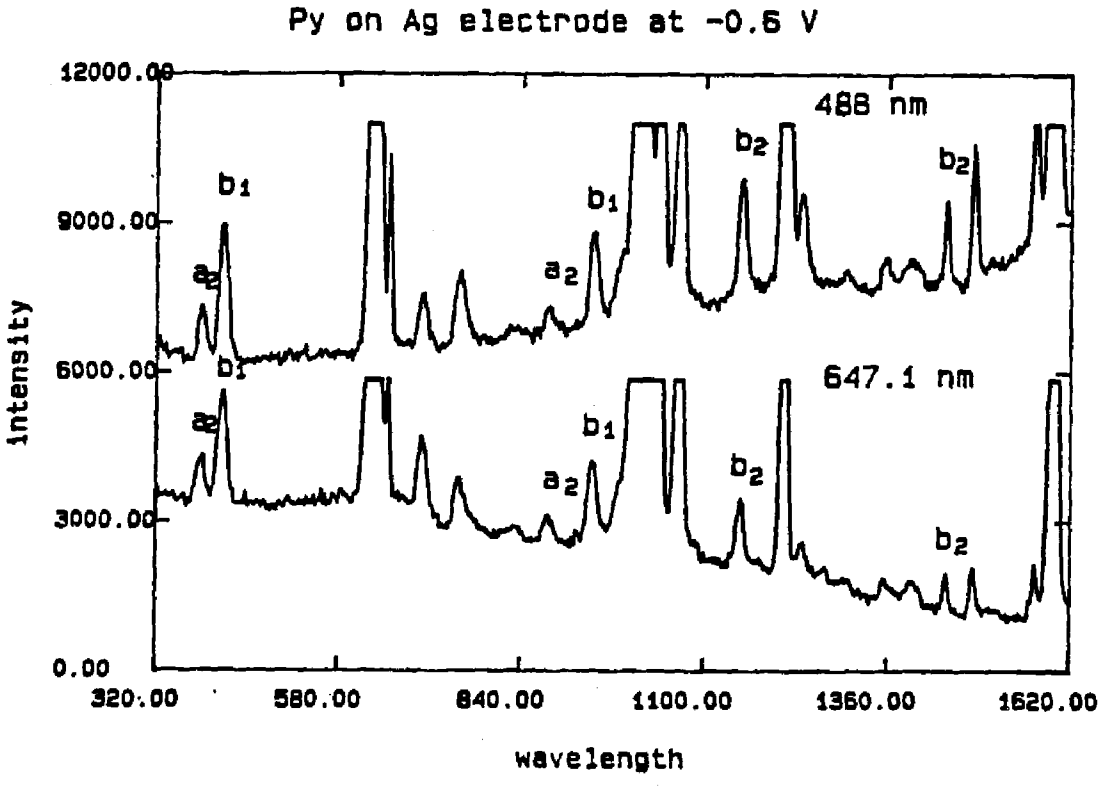

Figure 4-3. SERS spectra of pyridine on Ag electrode at −0.6 V vs SCE.

Table 4-2

SERS Intensity Ratios of Pyridine on the Ag Electrode at -0.6 V vs SCE

laser	$a_2 : b_1$		$b_2 : b_1$	
(nm)	$\frac{I_{383}}{I_{414}}$	$\frac{I_{879}}{I_{944}}$	$\frac{I_{1155}}{I_{944}}$	$\frac{I_{1444}}{I_{944}}$
488	0.40 ±0.01	0.29 ±0.02	1.43 ±0.05	0.96 ±0.01
647.1	0.41 ±0.01	0.29 ±0.02	0.85 ±0.01	0.47 ±0.00
$\frac{488}{647.1}$	0.98	1.00	1.60	2.04

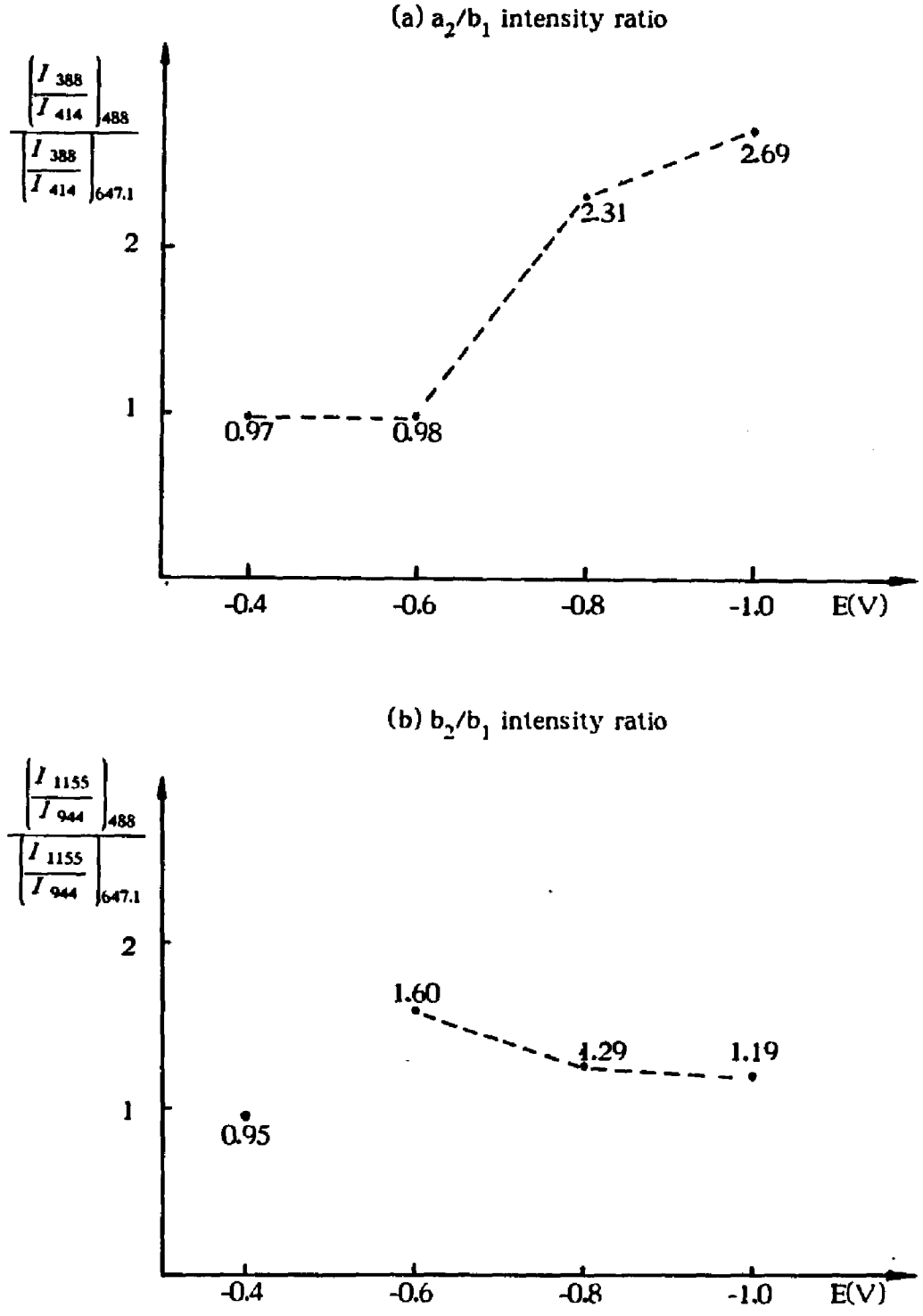

Figure 4-4. Potential dependence of intensity ratios of pyridine on the Ag electrode.

CHAPTER 5

SERS FROM FLAVINS ADSORBED ON A SILVER ELECTRODE

5.1 Introduction

The use of surface enhanced Raman scattering (SERS) spectroscopy for the study of biologically important molecules and other complex molecules is now well established [117]. The major advantages of SERS are its sensitivity which allows its use as an in situ method for examining molecules at interfaces and the quenching of fluorescence background which is often associated with complex molecules. The latter advantage is particularly important for the flavin molecules which fluoresce so strongly that resonance Raman (RR) spectra cannot be observed in solution without adding protein or KI as a quencher. The former attribute is utilized in this paper to study the surface Raman spectroscopy of flavin systems under electrode potential control.

A considerable number of resonance Raman studies have been made of flavins and flavoproteins with various methods [118-123] to conquer the difficulty of the fluorescence interference including two SERS studies on Ag colloids [124,125]. High quality spectra of flavoproteins [124] and free flavins [125] were obtained on silver colloidal particles upon the combination of fluorescence quenching and Raman intensity enhancement provided by the silver surface. The determination that adsorbed glucose oxidase in silver sol SERS experiments retains 86% of its enzymatic activity [124] suggests that SERS may be an extremely useful method for flavin Raman spectroscopy in biological systems. In order to further explore

the possibility of applying SERS for the study of flavin systems, we have carried out SERS measurements at silver electrodes which allows one to monitor flavin reduction reactions and obtain in-situ spectral information at the same time.

The flavin molecule is an important redox coenzyme which can be involved in single step two-electron processes for organic oxidation or reduction reactions or in two one-electron step processes for electron transfer to or from metal centers. The ability of flavins to operate in either mode is practically unique among biomolecules [126-128]. It is known that the tendency of the flavin toward one or two electron oxidation or reduction processes and the electrochemical potential of flavins are substantially affected by pH, by the polarity of the environment, and by interaction with metal ions. A study of these effects should reveal much about the methods open to proteins in controlling the reactivity of these coenzyme.

We have examined the electron transfer process of flavin reduction in different pH solutions with voltammetry and in-situ SERS spectroscopy. A spectrum, which was obtained from an acidic solution at the flavin reduction potential, was identified as being due to the semiquinone radical of the flavin. The semiquinone radical is formed by a single electron transfer and is an intermediate in the overall two-electron reduction. Cyclic voltammetry shows that the potential separation between the two single electron transfer steps changes with varying pH and the maximum value is about 50 mV. In such a case, electrochemical measurement cannot determine whether a twofold uptake of single electrons via an unstable intermediate or a single two electron reduction process occurs [129]. To our knowledge this is the first time that SERS spectroscopy has proved to be an effective approach for detecting unstable electrochemical intermediates at an electrode surface.

5.2 Experimental

Riboflavin (RF), flavin mononucleotide (FMN), flavin adenine dinucleotide (FAD) and D_2O were purchased from Sigma Chemical Co. and used as received. Reagent grade KNO_3, K_2SO_4, KCl and KBr served as supporting electrolytes. The solutions were prepared with deionized distilled water on the same day of the experiment and deaerated by nitrogen bubbling for twenty minutes. The pH of the solution was adjusted by adding reagent grade HNO_3 and NaOH and measured by an Orion Research digital ionalyzer model 801A.

The SERS experimental set up was similar to that described elsewhere [130]. A Spectra Physics 164 argon ion laser at 488 nm and 514.5 nm was used as an excitation source. Yellow or red light was obtained with a Spectra Physics Model 375 tunable dye laser. The laser power at the electrode was approximately 40 mW. Spectra were recorded with a Spex model 1401 double monochromater with a wavenumber resolution of around 4 cm^{-1}. Photon counting detection was used with an accumulation time of 0.6 s/cm^{-1}, and the intensities were recorded digitally and are presented unsmoothed.

The sample cell consisted of a silver working electrode with ca. 1.6 mm^2 surface area, a Pt counter electrode and a saturated calmel electrode (SCE) as the reference. All potentials in this paper are quoted vs SCE. The oxidation-reduction-cycle (ORC) pretreatment was accomplished in the presence of flavin molecules by applying a triangular sweep, 50 mV/s, from the initial potential to a switching potential of +0.25 V, +0.5 V and +0.6 V for KCl, K_2SO_4 and KNO_3 electrolytes, respectively. No difference in spectral features was observed from these three electrolyte solutions. Since the flavin is reduced at rather positive potentials in acidic solutions, we used K_2SO_4 in most cases in order to start electrode potential scans at

0.0 V. The ORC pretreatments were carried out in the dark and at neutral pH, and then the solution pH could be adjusted to a certain value by adding HNO_3 or NaOH solution. With yellow or red excitation the SERS spectrum could be observed when the flavin was added after an ORC pretreatment which was performed in a pure K_2SO_4 or KCl solution. In this case a flavin concentration higher than 10^{-5} M is required, while more intense spectra can be obtained from 10^{-7} M when the flavin is present during the ORC. When 488 or 514.5 nm excitation (in the absorption band) was used, it was found that a much better SERS spectrum could be obtained by eliminating the fluorescence from the flavin in the bulk solution by physically washing out the test solution with electrolyte blank after the ORC.

5.3 Results and Discussion

5.3.1 Surface Raman Spectra of Oxidized Flavin

Figure 5-1(A) shows the SERS spectrum of oxidized RF adsorbed at a roughened silver electrode at −0.4 V vs SCE when excited with 585 nm laser light. The solution contains 10^{-5} M RF and 0.1 M K_2SO_4 at a pH value of 6.8 for which the electrochemical reduction of RF occurs at an electrode potential more negative than −0.50 V vs SCE as found by cyclic voltammetry. Two other substituted flavins, FMN and FAD, exhibit the same SERS spectrum as RF, showing the side chain of the flavin is not involved in the surface enhancement. The SERS spectrum clearly reveals the same features of the flavin vibrational spectrum as the normal Raman (NR) spectrum [131].

The spectrum of Figure 5-1(C) was obtained under the same conditions as that for Figure 5-1(A) except that the excitation frequency was changed from 585 nm to 514.5 nm which is within the absorption band of the flavin. A 488-nm

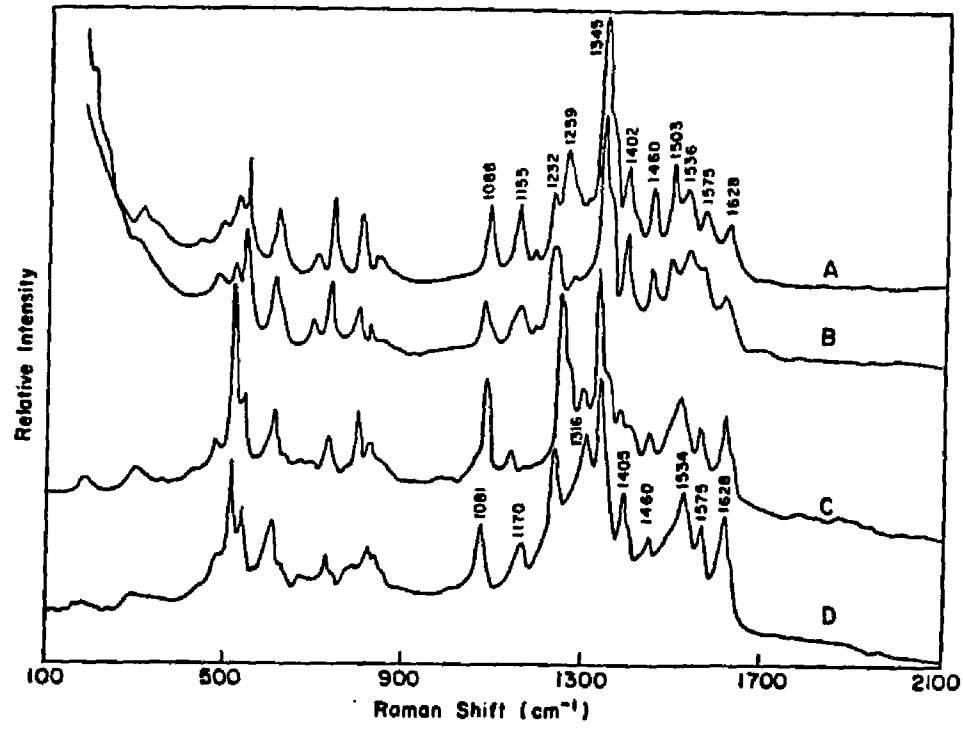

Figure 5-1. SERS and SERRS spectra of oxidized RF (10^{-5} M) on a Ag electrode in pH 6.8 (or pD 6.8) solution with 0.1 M K_2SO_4 as electrolyte at −0.4 V vs SCE. Excitation frequency 585 nm for (A) in H_2O and (B) in D_2O; 514.5 nm for (C) in H_2O and (D) in D_2O.

excitation gives exactly the same spectrum as Figure 5-1(C). In order to obtain these surface enhanced resonance Raman scattering (SERRS) spectra, the electrode was positioned within 4 mm of the cell window to reduce the fluorescence from the solution. It is possible to completely remove this fluorescence background by washing out the unadsorbed flavin molecules from the cell with pure electrolyte solution. This indicates a high fluorescence quenching efficiency of the surface interaction in contrast to quenching with a protein or KI. Furthermore, the spectrum taken after washing does not show any changes in band frequency or relative intensity with respect to the spectrum obtained before washing indicating that there is no RR component from the solution in the observed surface spectrum.

It can be seen that the 514.5-nm spectrum (Fig. 5-1(C)) is not greatly different from the 585-nm spectrum (Fig. 5-1(A)). However, several bands do show different relative intensities and there are also a few bands which shift in frequency. One possible explanation is that the Raman scattering processes are different and another possibility is that the RF undergoes a photochemical reaction to lumiflavin (the side chain of RF is broken and a CH_3 group is added) under 514.5-nm laser exposure (40 mw, 20 minutes). Lee *et al.* [125] found that with prolonged laser exposure (488 nm, 20 mw, 1 hour) on a silver sol system, a lumiflavin SERRS spectrum can be observed with a RF sample. In order to investigate whether there was photochemistry in our experiment, we first took a spectrum with 585-nm laser excitation followed directly with a second spectrum where the only change was the utilization of 514.5-nm excitation; and again obtained a third spectrum with 585-nm excitation under the same conditions. Each spectrum took ca. 20 minutes so that the three scans were completed in an hour. The first and the third spectra show exact agreement in both band frequencies and relative intensities and are identical to Fig. 5-1(A). The second spectrum is

different and appears as Fig. 5-1(C). These observations imply that the difference between the two spectra is due to a resonance effect rather than a photochemical reaction. This is supported by the parallel behavior of NR and RR spectra of the flavins (Table 5-1). Band VI and XIII shift down by ca. 7 cm^{-1} when the excitation is changed from the red into the resonance frequency in both solution and surface spectra. This can be explained by a different resonance enhancement effect on each vibrational mode. When an observed band is a composite of several overlapped vibrational modes, which is the case in flavin spectrum, a difference of 7 cm^{-1} in the two spectra is possible. Furthermore, the SERS and NR [131] spectra show similar features in their relative intensity pattern while the SERRS and RR [121] spectra are similar to each other despite some frequency shifts of the surface spectra from the solution spectra.

5.3.2 Spectral Analysis

The band frequencies of flavin SERS and SERRS spectra are listed in Table 5-1 along with the NR spectrum (obtained from 0.01 M FMN, 0.1 M K_2SO_4) and two reference RR spectra [120,121]. The assignments of Bowman *et al.* [132] and Schmidt *et al.* [120] are also listed in Table 5-1. Figure 5-2 shows the numbering of the atoms of the isoalloxazine ring which were used in the assignments. In the region of Raman shift from 1650 to 1000 cm^{-1}, all bands in SERS and SERRS have a one-to-one correspondence in frequency with those in the solution NR and RR spectra, respectively and do not shift with applied potential.

The bands at 1628, 1503, and 1460 cm^{-1} in the surface spectra, which involve the vibration of ring I only, do not show significant changes either in frequency or relative intensity compared with those in NR and RR spectra. This suggests that ring I is not involved in the surface interaction. Bands II and III, assigned to the

Table 5-1. Flavin Raman Frequency (cm^{-1}) and Assignment

band	Riboflavin on Ag electrode		FMN NR	RF(KI) RR[a]	RF(protein) RR[b]	Assigment[c]
label	585*	514.5	585	488	488	
I	1628m	1628s	1630m	1629s	1631s	νC_{5a}-C_6, νC_7-C_8, νC_8-C_9, νC_{5a}-C_{9a}
II	1575m	1575m	1583m	1582s	1584s	νC_{4a}-N_5,νN_{10}-C_{10a},νC_{10a}-N_1,νC_{4a}-C_{10a}
III	1536m	1535m	1550m	1547w	1548w	νC_{4a}-N_5, νC_{10a}-N_1
IV	1503s	1502m	1502s	1501m	1503m	δCH_3
V	1460m	1462w	1465m	1462w	1465w	νC_6-C_7, νC_8-C_9, νC_9-C_{9a}, δCH_3
		1416sh				
VI	1402s	1395m	1413s	1408s	1407s	νN_1-C_2, νC_{5a}-C_6, νC_8-C_9, νC_{5a}-C_{9a}
VII	1345vs	1344vs	1353vs	1353vs	1355vs	νN_{10}-C_{10a}, νC_{5a}-C_{9a}, δCH_3
VIII		1308w			1302w	νN_5-C_{5a},δCH_3
IX		1268sh		1277w	1282w	δCH_3, δN_3-H
X	1259s	1256vs	1260m	1256s	1252s	νC_{9a}-N_{10},δN_3-H,νC_6-N_1,δC_2=O,δC_4=O,δC_5-H,δC_6-H
XI	1232m		1231s	1228s	1229s	νN_3-C_4,νC_8-CH_3,δCH_3
XII	1186w		1187m	1182w	1179w	νN_1-C_2,νC_2-N_3,νN_3-C_4,νC_4-C_{4a},νC_{4a}-C_{10a},νC_7-CH_3,δCH_3
XIII	1155m	1147w	1167m	1157m	1161m	νC_2-N_3,νC_{4a}-C_4,νC_{4a}-C_{10a},νC_7-CH_3,δC_6-H
XIV	1088m	1088s	1080w		1073w	
XV	838w	833w			834m	
XVI	803m	804m	793m		789m	
XVII	740m	740m	752m		740m	
XVIII	618m	617m	615w		633m	
XIX	551s	553m	544w		605m	
XX	532m	529s			521m	
XXI	493w	492w			496m	
XXII	305w	312w			303w	
XXIII	194w	196w				

(a) ref. 120, (b) ref. 121, (c) ref. 132 and 120.

* excitation frequency (nm)

vs--very strong; s--strong; m--medium; w--weak; sh--should

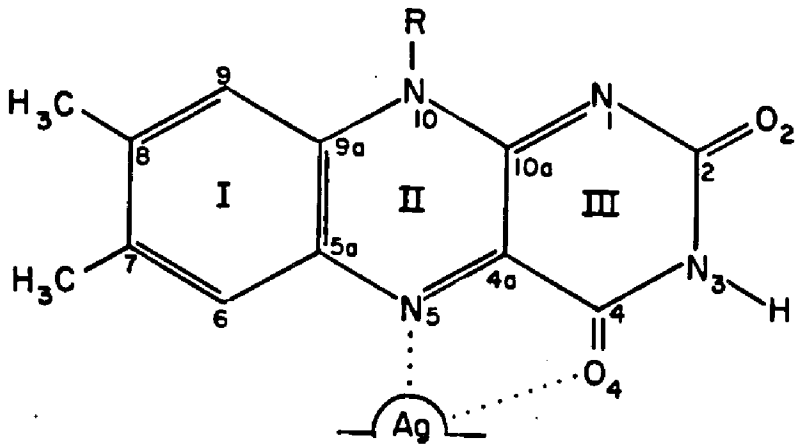

Figure 5-2. Surface complex structure and numbering of the isoalloxazine ring of the falvin.

stretching vibration of the N_5 =C_{4a}-C_{10a}=N_1 conjugated bond, were shifted down from the NR and RR spectra, indicating that N_5=C_{4a}-C_{10a}=N_1 atoms are likely involved in the binding between flavin molecule and silver surface. Moreover, another two bands numbered VI and VII, which shift to lower frequencies, can be assigned to the vibrations associated with one of those four atoms as well. Band X is well known and is characteristic of the N_3-H bending motion. It disappears in the FAD^- anion CARS spectrum [133] and shifts up by about 40 cm^{-1} upon the N_3 deuteration [118,121]. The presence of this band in our surface spectra indicates that the adsorbed flavin molecules are N_3 protonated. The band labeled XI at 1232 cm^{-1} is associated with the N_3-C_4 stretching vibration modes and does not shift in SERS on the Ag electrode, implying no surface interaction at the N_3 atom. The relative intensity of band XII at 1186 cm^{-1} decreases and band XIII shifts down by ca. 10 cm^{-1} upon the surface interaction with Ag electrode. Since these bands involve the vibrations related to C_2, N_3, C_4, C_{4a} and C_{10a} atoms, both N_5, O_4 surface bonding or N_3 surface bonding may account for these changes. However, all the facts mentioned above can be interpreted in terms of an interaction between flavin and the silver electrode surface at N_5 and O_4 (Fig. 5-2). The effect of the interaction spreads to C_4, C_{4a}, C_{10a} and N_1 along the conjugation pathway so that all related bands change in surface spectra either in band position or relative intensity.

Spectra (B) and (D) in Figure 5-1 were obtained from D_2O solution where the N_3-H is deuterated in the SERS and SERRS spectra. As in the case of solution Raman studies the change occurs in the 1300-1100 cm^{-1} region (Table 5-2). In the solution Raman spectra, band X shifts about 40 cm^{-1} to higher frequency, which is interpreted as the result of a decrease in the N_3-H bending character after deuteration leading to an up-shift toward the intrinsic frequency of the C=O

Table 5-2. Flavin N_3-H(D) Isotopic Frequency Shifts

	Riboflavin on Ag electrode				FMN		RF(protein)		RF(Ag sol)	
band	SERS(585*)		SERRS(514.5)		NR[a](600)		RR[b](488)		SERRS[c](488)	
label	H_2O	D_2O	H_2O	D_2O	H_2O	D_2O	H_2O	D_2O	H_2O	D_2O
I	1628m	1628m	1628s	1628s	1633m	1628m	1631s	1630s	1630vs	1630vs
II	1575m	1575m	1575m	1575m	1584m	1584m	1584s	1582s	1576m	1577m
III	1536m	1538m	1535m	1534m	1551m	1548m	1548w	1548w	1536w	1536m
IV	1503m	1502m	1502m	1500sh	1503m	1502m	1503m	1499m	1507m	1507m
V	1460m	1458m	1462w	1460w	1469m	1468m	1465w	1462w	1465w	1465w
			1416sh				1420sh	1420sh		
VI	1402s	1403s	1395m	1405m	1413s	1411s	1407s	1406s	1409m	1409m
VII	1345vs	1348vs	1344vs	1348vs	1355vs	1351vs	1355vs	1351vs	1349vs	1350vs
VIII			1308w				1302w		1308sh	1309sh
IX			1268sh		1282w					
X	1259s	1281w	1256vs	1316m	1261m	1300w	1252s	1295s	1287s	1289s
XI	1232m	1242m		1244s	1233s	1230m	1229s	1232w	1235m	1246m
XII	1186w	1188w			1187m	1172m	1179w	1181w	1190w	1190w
XIII	1155m	1172m	1147w	1170m	1166m	1148m	1161m	1147m	1160m	1163m
XIV	1088m	1084m	1088s	1081s				1138m	1092m	1090m

(a) ref. 131, (b) ref. 121, (c) ref. 125.

* excitation frequency (nm)

vs--very strong; s--strong; m--medium; w--weak; sh--shoulder

vibrations [134]. In our surface spectra this band also disappears from the 1259 cm^{-1} region. However, the new band appears weakly at 1281 cm^{-1} in the D_2O SERS spectrum, while it seems to be overlapped at 1316 cm^{-1} with the 1303 cm^{-1} band in the D_2O SERRS spectrum. Neither of these bands can be assigned in certainty. Nevertheless, the unambiguous isotopic effect in the 1300-1100 cm^{-1} region is in sharp contrast to the identical SERRS spectra from H_2O and D_2O in Ag sol experiments [125] (Table 5-2) where the N_3 deprotonated anion was found to be the SERS active species. Furthermore, the authors [125] found that making the Ag colloidal solution acidic produces gradual attenuation with an abrupt loss of signal around pH 4, while we observed the SERS and SERRS spectra of flavins at pH 2 with about equal intensity as observed in the pH 7 solution both at 0 V vs SCE. The N_3 protonated neutral flavin is thus suggested to be the SERS active species on the Ag electrode which probably has a different surface charge than the silver colloidal particles. The difference in protonation state of the SERS active species on the electrode and sols is clearly reflected in the surface spectra where band X shifts up in Ag sols by ca. 35 cm^{-1} from its position in the solution RR spectrum, while it remains virtually unchanged on Ag electrodes (Table 5-2). Here we see an example of the phenomenon that SERS results on Ag electrodes may show differences from analogous results on Ag sols because the surface charge can be different in the two cases depending on the experimental conditions.

5.3.3 SERRS spectrum of Semiquinone Radical

Figure 5-3(A) shows a SERS spectrum of FMN obtained with 602.4 nm excitation in pH 4.5 solution at −0.3 V vs SCE where the flavin reduction occurs. Some new bands appeared with a concomitant intensity decrease of those known bands corresponding to the oxidized flavin when the potential was changed from

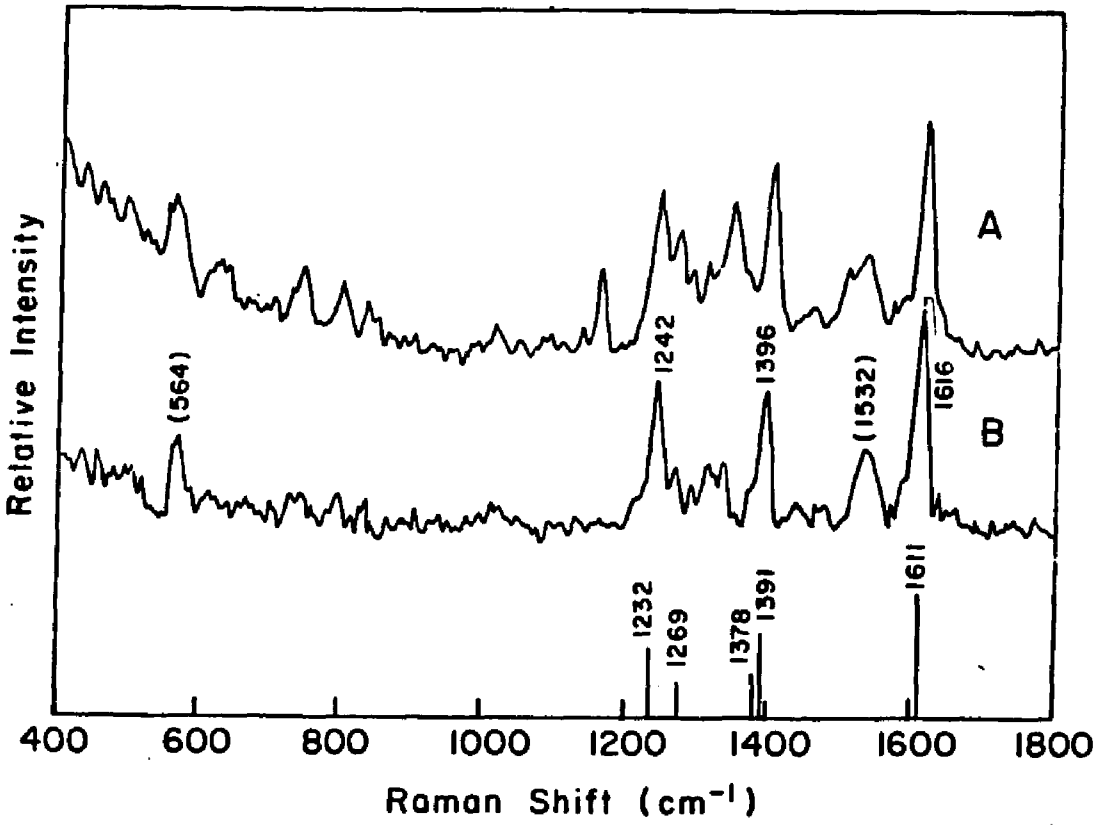

Figure 5-3. SERRS spectrum of semiquinone flavin obtained in pH 4.5 solution at −0.3 V vs SCE with excitation frequency of 602.4 nm. (A) is the recorded spectrum; in (B) the Raman bands of the oxidized flavin are subtracted out from the spectrum (A). The straight lines at the bottom are labels of Raman bands of Clostridium MP-flavodoxin in the neutral semiquinone form obtained by CARS [123].

−0.1 V to −0.3 V. To isolate the bands due to the new species, a spectrum obtained at −0.1 V where only oxidized flavin exists was multiplied by a factor of 0.4 so that most oxidized bands have a similar intensities with those at −0.3 V. It was then subtracted from Figure 5-3(A), giving the spectrum of Figure 5-3(B) attributable to the new species. Since this spectrum disappeared when the potential was more negative than −0.5 V vs SCE where the flavin is fully reduced in a pH 4.5 solution, it is apparent that fully reduced flavin is not responsible for the new spectrum. It was at first sight surprising that no SERS spectrum of reduced flavin was observed with yellow-red excitation. This observation cannot be explained by the lack of resonance enhancement (reduced flavin is colorless) since the oxidized flavin does not absorb light in this frequency region as well. However, the N_5 and N_1 of the isoalloxazine ring are protonated upon the reduction leading to a non-planar configuration of the molecule. The loss of both nitrogen lone pairs and conjugated π orbitals, which are generally responsible for the chemisorption of SERS molecules, may account for the absence of reduced flavin SERS spectrum. Thus the flavin semiquinone radical, the intermediate of two single electron transfer reduction, is proposed for the new spectrum. For comparison, the band positions and relative intensities of Clostridium MP flavodoxin semiquinone in aqueous solution observed by CARS [125] are presented by the straight lines at the bottom of the Figure 5-3.

With the exception of a band at 1532 cm^{-1}, bands in Figure 5-3(B) at frequencies above 1000 cm^{-1},(CARS spectrum is not available below 1000 cm^{-1}), correspond to those in the solution Raman spectrum of the semiquinone with only slight frequency shifts. The relative intensity of the 1532 cm^{-1} band of the oxidized flavin increases at more negative potentials. Therefore, this was not subtracted out as were other bands of the oxidized flavin. Three other bands at 1616,

1396 and 1242 cm^{-1} are identified as surface spectral bands of the neutral semiquinone adsorbed on the Ag electrode (Figure 5-3B).

Three ionized forms of the semiquinone flavin (anion, neutral, and cation) may exist in solution. (Figure 5-4) The pH range for observing the SERS spectrum of Figure 5-3(B) is from 2 to 7 consistent with the acid dissociation property of the flavin semiquinone radical. The pKa value for the cation is ca. 1.3 and for neutral radical it is 6.5 so that neutral semiquinone is the major component in pH 2-7 solution [136,137]. It is known that neutral flavin radical has a blue color with ϵ_{max} at about 580 nm [133]. Thus, the spectrum obtained with 602.4-nm exciting light (within the absorption band) is actually a SERRS spectrum. In solution a single band at ca. 1616 cm^{-1} is observed with 488-nm laser excitation within the second absorption band of flavin radical (ϵ_{max} is at about 510 nm) [133]. However, it does not appear in the surface spectrum excited with 488- or 514.5-nm laser light possibly due to the destabilization of surface semiquinone species by a photoeffect.

At pH above 6.5 (the pKa value of neutral semiquinone radical), the flavin semiquinone anions are the major species of the radical intermediate. In repeated attempts we could not observe any new bands at flavin reduction potentials from −0.5 to −0.7 V in pH 8-12 solutions with excitation frequencies from 488 to 647.1 nm. The SERS spectrum from oxidized flavin disappears at potentials more negative than −0.7 V vs SCE. It should be noted that this potential is well positive to the potential at which the loss of SERS active sites begins. Thus no evidence for the existence of semiquinone anion intermediate was observed by SERS.

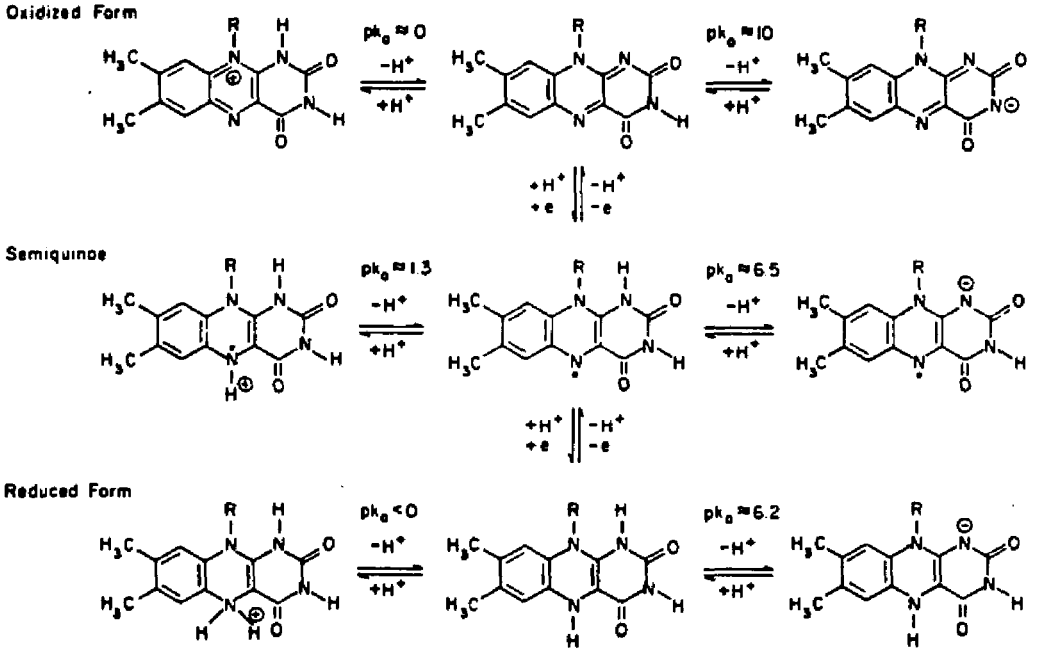

Figure 5-4. Flavin redox system and occurrence of the flavin species as a function of pH and redox state (adapted in the manner of Dryhurst [136], from Hemmerich et al. [137] and Janik et al. [138]).

5.3.4 Electron Transfer Process of Flavin Reduction on a Silver Electrode

Cyclic voltammetry (CV) was carried out in 1 mM FMN and 0.1 M K_2SO_4 solution with pH values in the range 2-12. Three typical cyclic voltammetric curves obtained on a SERS pretreated (rough) silver electrode at various pH values are shown in Figure 5-5. At pH 4.2-4.6, there are two distinguishable waves in the CV curve (Fig. 5-5B). The peak currents are proportional to the square root of the sweep rate (4-400 mV/s) indicating that both waves are diffusion controlled and thus a two one-electron transfer process is suggested. At pH 2-4.2 (Figure 5-5A), the CV curve is similar to the case of two single electron transfer with over-lapped potentials [129]. At pH above 4.6, the single peak in the CV curves is quite broad probably due to the mixing of multiple processes since the neutral and anion form of the redox species have different reduction potentials.

The observation of the semiquinone intermediate in pH 2-7 solution by SERRS spectra enable us to conclude that the flavin is electrochemically reduced on a rough silver electrode via two one-electron steps in acidic solution although the potential separation is rather small or even overlapped. Both a polished (smooth) Ag electrode and a pretreated (rough) Ag electrode show CV curves with two diffusion controlled waves at pH 4.5. This is consistent with the formation of the semiquinone intermediate on the smooth as well as on the rough Ag electrode. The similarity of the dual CV peaks at pH 4.5 on both types of Ag electrodes shows that the same reduction mechanism occurs at the two electrode surfaces. This CV morphology only occurs over the narrow pH range of 4.2 to 4.6 where the most intense semiquinone spectrum is observed. Much weaker spectra for the semi-quinone intermediate are found in the pH 2-4 and 5-7 regions where the CV

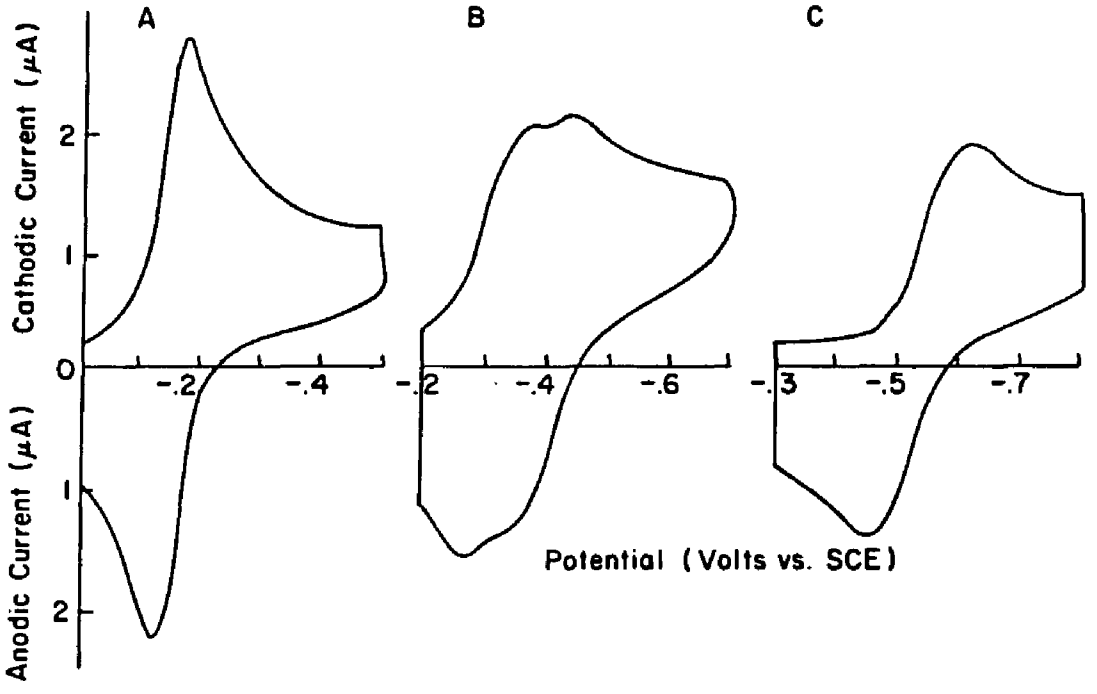

Figure 5-5. Cyclic voltammetric curves for FMN (1 mM) on a rough Ag electrode with 0.1 M K_2SO_4 as the electrolyte. (A) pH 2.0; (B) pH 4.5; (C) pH 9.0. The scan rate is 20 mV/s.

curves only show one peak. Although the spectral data do not prove a two step charge transfer mechanism in these pH regions for the smooth Ag electrode, the fact that the SERS and CV curves establishes the existence of the intermediate strongly suggests that a two step mechanism involving overlapped reduction potentials takes place on both types of electrode surface over the entire pH 2-7 region.

5.4 Conclusion

The observation of the semiquinone intermediate by surface Raman spectroscopy combined with the well defined CV curves obtained on SERS activated Ag electrodes demonstrates the utility of this electrode system for the study of electrochemical processes. Additionally, we find only a weak perturbation of the flavin electronic and redox properties upon adsorption as indicated by the similarity of the SERRS spectrum with the free flavin RR spectrum and by the results of the cyclic voltammetry on the smooth and rough Ag electrode. Thus the possibility of an enzymatically active flavoprotein adsorbed at a Ag electrode surface, as has been proposed on Ag colloids by Copeland et. al. [124], is not ruled out by the proposed bonding sites for the flavin on a SERS active Ag electrode. Presumably, the surface binding is weak enough so that a biological substrate, e. g., glucose, could compete favorable for the enzymatically active site at the N_5 atom.

REFERENCES

1. Chem. & Eng. News, Aug. 11, 1986, p22.
2. Frotzeim, H., In "Topic in Current Physics, Vol. 4", Springer-Verlag, New York, 1977, p205.
3. Bowker, M. and Madix, R. J., Surf. Sci., 1980, 95, 190.
4. Ducros, R.; Alnot, M; Ehrhardt, J. J.; Housely, M; Piquard, C. and Cassuto, A., Surf. Sci., 1980, 94, 154.
5. Johnson, W. G. and Heldt, L. A., J. Electrochem. Soc., 1974, 121, 34.
6. Slusser, G. J. and Winograd, N, Surf. Sci., 1980, 95, 53.
7. Fleisch, T.; Winograd, N and Delegass, W. N, Surf. Sci., 1978, 78, 141.
8. Fleischman, M; Hendra, P. J. and McQuillan, A. J., Chem. Phys. Lett., 1974, 26, 123.
9. Jeamaire, D. L. and Van Duyne, R. P., J. Electroanal. Chem., 1977, 84, 1.
10. Albrecht, M G. and Creighton, J. A., J. Am. Chem. Soc., 1977, 99, 5215.
11. Crighton, J. A.; Blatchford, C. G. and Albrecht, M G., J. Chem. Soc. Faraday Trans. 2, 1979, 75, 790.
12. Lippitsch, M E., Chem. Phys. Lett., 1980,74(1), 125.
13. Wood, T. H. and Klein, M V., J. Vac. Sci. Technol., 1979, 16, 459.
14. Rowe, J. E.; Snank, C. V.; Zwemer, D. A. and Murray, C. A., Phys. Rev. Lett., 1980, 44(26), 1770.
15. Tsang, J. C.; Kirtley, J. R. and Bradley, J. A., Phys, Rev. Lett., 1979, 43, 772.
16. Tsang J. C. and Kirtley, J., Solid State Commun., 1979, 30(10), 617.
17. Murray, C. A. In "Recant Advances in Laser Spectroscopy, Vol. 3", Eds. Garetz, B. A. and Lombardi, J. R., John Wiley and Sons, New, York, 1986, p24.
18. Furtak, T. E. and Reyes, J., Surf. Sci., 1980, 93, 351.
19. Birke, R. L. and Lombardi, J. R., In "Advances in Laser Spectroscopy, Vol. 1", Eds. Garetz B. and Lombardi, J. R., Heydon and Sons, London, 1982, p143.
20. Birke, R. L.; Lombardi, J. R. and Sanchez, L. A., In "ACS Advances in Chemistry Series, Vol. 201", Ed. Kadish, K. M, Am. Chem. Soc., 1982, p201.
21. "Surface Enhanced Raman Scattering", Eds. Chang, R. K. and Furtak, T. E., Plenum Press, New York, 1982.
22. Otto, A. In "Light Scattering in Solids, Vol. IV", Eds. Cardona, M and Gunth-

erodt, G.; Springer-Verlag, Berlin, 1984.

23. Chang, R. K. and Laube, B. L. In "CRC Critical Reviews in Solid State and Materials Sciences, Vol. 12", CRC Press Inc., 1984, p1.

24. Campion, A., Ann. Rew. Phys. Chem. 1985, 36, 549.

25. King, F. W.; Van Duyne, R. P. and Schatz, G. C., J. Chem. Phys., 1978, 69, 4472.

26. Schatz, G. C. and Van Duyne, R. P., Surf. Sci., 1980, 101, 425.

27. Efrima, S. and Metiu, H., Israel J. Chem., 1979, 18, 17.

28. Besley, G. L. and Smith, J. R. Solid State Commun., 1979, 31, 815.

29. Morawitz, H. and Koehler, T. R., Chem. Phys. Lett., 1980, 71, 64.

30. Campion, A.; Gallo, A. R.; Harris, C. B.; Robota, H. J. and Whitmore, P. M, Chem. Phys. Lett. 1980, 73, 447.

31. Schatz. G. C. In "Surface Enhanced Raman Scattering", Eds. Chang, R. K. and Furtak, T. E.; Plenum Press, New York, 1982, p35.

32. Ford, G. W. and Weber, W. H., Surf. Sci., 1981, 109, 451.

33. Hilton, P. R. and Oxtoby, D. W., J. Chem. Phys., 1980, 72, 6346.

34. Pondey, P. K. and Schatz, G. C., Chem. Phys. Lett., 1982, 88, 193.

35. Korzeniewski, G.; Maniv, T. and Metiu, H., Chem. Phys. Lett., 1980, 73, 212.

36. Maniv, T. and Metiu, H., J. Chem. Phys., 1980, 72, 1996.

37. Feibelman, P. J., Phys. Rew. B, 1975, 12, 1319.

38. Weber, W. H. and Ford, G. W., Phys. Rev. Lett., 1980, 44, 1774.

39. Lee, T. K. and Birman, J. L., Phys. Rew. B, 1980, 22, 5953.

40. McCall, S. L. and Platzman, P. M, Phys. Rew. B, 1980, 22, 1660.

41. Otto, A.; Timper, J.; Billman, J.; Kovacs, G. and Pockrand, I., Surf. Sci., 1980, 92, L55.

42. Maniv, T. and Metiu, H., Chem. Phys. Lett., 1981, 79, 79.

43. Raether, H. In "Physics of Thin Films", Eds. Hass, G; Francombe, M. and Hoffman, R., Academic Press, New York, 1977, p145.

44. Simon, H. J.; Mitchell, D. E. and Watson, J. G., Am. J. Phys., 1975, 43, 630.

45. Maraduddin, A. A. and Mills, D. L., Phys. Rew. B, 1975, 11, 1392.

46. Celli V. and Marvin, A., Phys. Rew. B, 1975, 11, 1779.

47. Chen, Y. J. and Chen, W. P. and Burstein, E., Phys. Rew. Lett., 1976, 36, 1207.

48. Sakoda, K.; Ohtaka, K. and Hanamura, E., Solid State Commun., 1982, 41, 393.

49. Weber, W. H. and Ford, G. W., Optics Lett., 1981, 6, 122.

50. Sanda, P. N; Warlaumon, J. M; Demuth, J. E; Tsang, J. C.; Christman, K. and Bradley, J. A., Phys. Rew. Lett., 1980, 45, 1519.

51. Girlando, A.; Philpott, M. R.; Heitman, D.; Swalen, J. D. and Santo, R., J. Chem. Phys., 1980, 72, 5187.

52. Jha, S. S.; Kitley, J. R. and Tsang, J. C., Phys. Rev. B, 1980, 22, 3973.

53. Arya, K.; Zeyher, R. and Maradudin, A. A., Solid State Commun., 1982, 42, 461.

54. Aravind, P. K. and Metiu, H. Chem. Phys. Lett., 1980, 74, 301.

55. Chen, C. Y.; Davoli, I.; Ritchie, G. and Burstein, E., Surf. Sci., 1980, 101, 363.

56. Burstein, E.; Chen, C. Y. and Lundquist, S., In "Light Scattering in Solids", Eds. Birman, J. I.; Cummins, H. Z. and Rebane, K. K., Plenum Press, New York, 1979, p479.

57. Dornhaus, R.; Benner, R. E.; Chang, R. K. and Chabay, I., Surf. Sci., 1980, 101, 367.

58. Pettinger, B.; Tadjeddine, A. and Kolb, D. M., Chem. Phys. Lett., 1979, 66, 544.

59 Tom, H. W. K.; Chen, C. K.; de Castro, A. R. B. and Shen, Y. R., Solid State Commun., 1982, 41, 259.

60. Wenning, U.; Pettinger, B. and Wetzel, R. P., Chem. Phys. Lett., 1980, 70(1), 49.

61. Pettinger, B.; Wenning, U. and Wetzel, H., Surf. Sci., 1980, 101(1-3), 409.

62. Pettinger, B.; Wenning, U. and Wetzel. H., Chem. Phys. Lett., 1979, 67(1), 192.

63. Campion, A. and Mullins, D. R., Chem. Phys. Lett., 1983, 94(6), 576.

64. Schultz, S. C.; Janik-Czachor, M. and Van Duyne, R. P., Surf. Sci., 1981, 104, 419.

65. Evans, J. F.; Albrecht, M. G.; Ullevig, D. M. and Hexter, R. M., J. Electroanal. Chem., 1980, 106, 209.

66. Creighton, J. A.; Blatchford, C. G. and Albrecht, M. G., J. Chem. Soc. Faraday Trans. II, 1979, 75 790.

67. Chen, C. Y.; Burstein, E. and Lundquist, S., Solid State Commun., 197, 32, 63.

68. Chen, C. Y. and Burstein, E., Phys. Rev. Lett., 1980, 45, 1287.

69. Murray, C. A.; Allara, D. L.; Hebard, A. F. and Padden, F. J., Jr, Surf. Sci., 1982, 119, 49.

70. Liao P. In "Surface Enhanced Raman Scattering", Eds. Chang, R. K. and Furtak, T. E., Plenum Press, New York, 1982, p379.

71. Kerker, M; Wang, D.-S. and Chew, H., Appl. Optics, 1980, 19, 4159.

72. Gersten, J. I. and Nitzan. A., J. Chem. Phys., 1980, 73, 3023.

73. Adrian, F. J., Chem. Phys. Lett., 1981, 78, 45.

74. McCall, S. L; Platzman, P. M. and Wolff, P. A., Phys. Lett., 1980, 77A, 381.

75. Jackson, J. D. In "Classical Electrodynamics", John Wiley & Sons, New York, 2nd Ed., 1975, p150.

76. Johnson, P. B. and Christy, R. W., Phys. Rev., 1972, B6, 4370.

77. Hagemann, H.-J.; Gudet, W. and Kunz, C., J. Opt. Soc. Am., 1975, 65, 742.

78. Barber, P. W.; Chang R. K. and Massoudi, H., Phys. Rev. Lett., 1983, 50, 997.

79. Barber, P. W.; Chang, R. K. and Massoudi, H., Phys. Rev. B, 1983, 27, 7251.

80. Moskovits, M. and DiLella, D. P., p243 in Ref. 21.

81. Jeanmaire, D. L. and Van Duyne, R. P., J. Electroanal. Chem., 1977, 84, 1.

82. Bunding, K.; Birke, R. L. and Lombardi, J. R., Chem. Phys., 1980, 54, 115.

83. Roy, D. and Furtak, T. E., Chem. Phys. Lett., 1985, 124(4), 299.

84. Fleischmann, M; Hendra, P. J.; Hill, I. R. and Pemble, M. E., J. Electroanal. Chem., 1981, 117, 243.

85. Wood, T. H. and Kelin, M. V., Solid State Commun., 1980, 35, 263.

86. Wood, T. H., Phys. Rev. B24, 1981, 2289.

87. Van Duyne, R. P., In "Chemical and Biochemical Applications of Laser, Vol. 4", Ed. Moore, C. B., Academic Press, 1979, p101.

88. Birke, R. L; Lombardi, J. R. and Gersten, J. I., Phys. Rev. Lett., 1979, 43, 71.

89. Wetzel, H. A.; Gerischer, H. and Pettinger, B., Chem. Phys. Lett., 1981, 80, 392.

90. Marinyuk, V. V.; Lazorenko-Manevich, R. M. and Kolotyrkin, Ya-M., In " Advance in Physical Chemistry", Ed. Kolotyrkin, Ya. M., MIR Publishers, Moscow, 1982, p148.

91. Watanabe, T.; Yangihara, N; Honda, K.; Pettinger, B. and Moerl, L., Chem. Phys. Lett., 1983, 96, 649.

92. Furtak, T. E. and Roy, D., Phys. Rev. Lett., 1983, 50, 1301.

93. Moerl, L. and Pettinger, B., Solid State Commun., 1982, 43, 315.

94. Furtak, T. E. and Macoomber, S. H., Chem. Phys. Lett., 1983, 95, 328.

95. Billman, J. and Otto, A., Solid State Commun., 1982, 44, 105.

96. Otto, A., J. Electron Spectrosc. Relat. Phenon., 1983, 29, 357.

97. Billman, J. and Otto, A., Surf. Sci., 1984, 138, 1.

98. Lombardi, J. R.; Birke, R. L.; Sanchez, L. A.; Bernard, I. and Sun, S. C., Chem. Phys. Lett., 1984, 104, 240.

99. Demuth, J. E. and Sanda, P. N, Phys. Rev. Lett., 1981, 47, 57.

100. Otto, A.; Frank, K. H. and Reihl, B., preprint.

101. Gersten, J. I.; Birke, R. L. and Lombardi, J. R., Phys. Rev. Lett., 1979, 43, 147.

102. Burstein, E.; Chen, Y. J.; Landquist, S. and Tosatti, E., Solid State Commun., 1979, 21, 567.

103. King, F. W. and Schatz, G. C., Chem. Phys., 1979, 32, 245.

104. Persson, B. N. J., Chem. Phys. Lett., 1981, 82(3), 561.

105. Rowe, J. E.; Shank, C. V.; Zwemer, D. and Murray, C. A., Phys. Rev. Lett., 1980, 44, 1770.

106. Albrecht, A. C., J. Chem. Phys., 1961, 34. 1476.

107. Tang, T. and Albrecht, A. C., In "Raman Spectroscopy, Theory, and Practice, Vol 2", Ed. Szymanski, H. A., Plenum, New York, 1970, p33.

108. Adrian, F. J., J. Chem. Phys., 1982, 77, 5302.

109. Sanchez, L.; Lombardi, J. R. and Birke, R. L., J. Phys. Chem., 1984, 88. 1762.

110. Lippitsch, M. E., Phys. Rev., 1984, B29, 3101.

111. Takahashi, M; Goto, M. and Ito, M, Chem. Phys. Lett., 1985, 121(4,5), 458.

112. Pettinger, B., Chem. Phys. Lett., 1981, 78, 404.

113. Lombardi, J. R.; Birke, L. R.; Lu, T. and Xu, J., I Chem Phys., 1986, 84(8), 4174.

114. Birle, R. L.; Bernard, I.; Sanchez, L. A. and Lombardi, J. R., J. Electroanal. Chem., 1983, 150, 447.

115. Crighton, I. A., Surf. Sci., 1983, 124, 209.

116. Moskovits, M. and Suh, J. S., J. Phys. Chem., 1984, 88, 5526.

117. Cotton, T. M. In "Surface and Interfacial Aspects of Biomedical Polymers, Vol. II", Anderade, J. B. Ed.; Plenum Press: 1985, p161.

118. Dutta, P. K.; Nestor, J. R. and Spiro, T. G. Proc. Natl. Acad. Sci. U.S.A. 1977,76,4146-4149.

119. Nishina, Y.; Kitagawa, T.; Shiga, K.; Horiike, K.; Matsumura, Y.; Watari, H.

and Yamano, T. J. Biochem. (Tokyo) 1978,84,925-932.

120. Schmidt, J.; Coudron, P.; Thompson, A. W.; Watters, K. L. and McFarland, J. T. Biochem. 1983, 22, 76-84.

121. Kitagawa, T.; Nishina, Y.; Kyogoku, Y.; Yamano, T.; Ohishi, N.; Takai-suzuki, A. and Yagi, K. Biochem. 1979, 18 (9) 1804-1808.

122. Schopfer, L. and Morris, M. Biochem. 1980, 19, 4932.

123. Schopfer, L.; Haushlter, J.; Smith, M.; Milad, M. and Morris, M. Biochem. 1981, 20, 6734-6739.

124. Copeland, R. A.; Fodor, S. P. A. and Spiro, T. G. J. Am. Chem. Soc. 1984, 106, 3872-4.

125. Lee, N. S.; Sheng, R. S.; Morris, M. D. and Schopfer, L. M., J. Am. Chem. Soc., 1986, 108, 6179-6183.

126. Hemmerich, P. In "Bioinorganic Chemistry II"; Raymond, K. N. Ed.; American Chemical Society: Washington, D.C., 1977; p312.

127. Hemmerich, P.; Massey, V. In "Oxidases and Related Redox Systems"; King, T. E.; Mason, H. S.; Morrison, M. Eds.; Pergamon Press: Oxford, 1979.

128. Walsh, C. Acc. Chem. Res. 1980, 13, 148-155.

129. Bard, A. J. and Faulkner, L. R. "Electrochemical Methods" John Wiley and sons, Inc. New York, 1980, p232-236.

130. Birke, R. L.; Lombardi, J. R. and Sanchez, L. A. "Surface Enhanced Raman Spectroscopy", in Advances in Chemistry Series No. 201, Chap.4 Ed. Kadish, K. M. Am. Chem. Soc., 1982.

131. Nisihmura, Y. and Tsuboi, M. Chem. Phys. Lett. 1978, 59 (2) 210-213.

132. Bowman, W. D. and Spiro, T. G. Biochem. 1981, 20, 3313-3318.

133. Dutta, P. K.; Spencer, R.; Walsh, C. and Spiro, T. G. Biochim. Biophys. Acta, 1980, 623, 77-83.

134. Dutta, P. K.; Nestor, J. and Spiro, T. G., Biochem. Biophys. Res. Commun., 1978, 83(1), 209-216.

135. Dutta, P. K. and Spiro, T. G. Biochem. 1980,19,1590-1593.

136. Dryhurst G. In "Electrochemistry of Biological Molecules"; Academic Press, Inc.: New York, 1977; p371.

137. Hemmerich, P.; Veeger, C. and H.C.S. Wood, A. Chem. Int. Ed Engl. 1965, 4, 467.

138. Janik, B. and Elving, P. J. Chem. Rev. 1968, 68, 295.